3.3.1 Derivation of the MVIV model

3.3.1.1 MVIV model set-up

The MV to IV model consists of one manipulated variable, casting speed ($u(t)$) and two measured disturbances, mould level ($d_1(t)$) and inlet temperature ($d_2(t)$). The outputs consist of 38 thermocouple temperatures ($\mathbf{y}(t) = [y_1(t) \quad y_2(t) \quad \dots \quad y_{38}(t)]^\top$). A block diagram depicting the MV to IV model is shown in Fig. 3.12. For the system identification procedure,

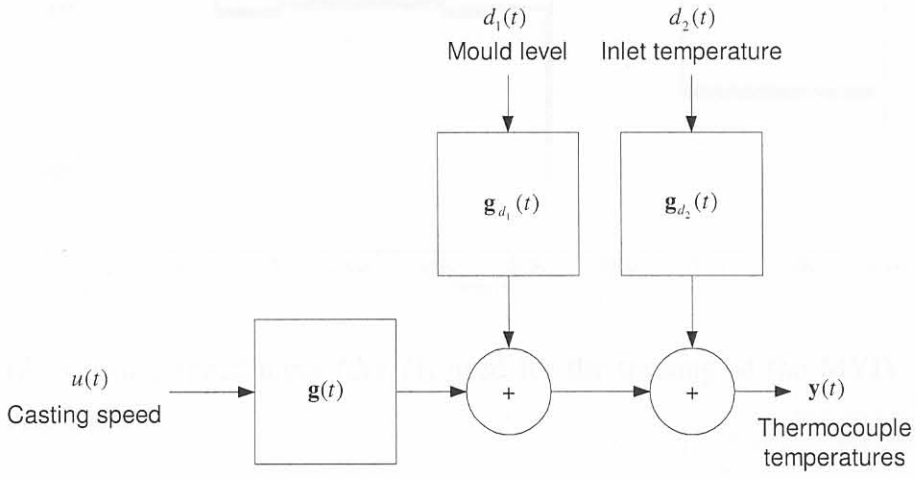

Figure 3.12 Block diagram depiction of the MV to IV model showing, manipulated variable, disturbances and output variables.

casting speed, mould level and inlet temperatures are inputs (*i.e.* $m = 3$ in §2.2.4). The thermocouple temperatures are the outputs (*i.e.* $p = 38$ in §2.2.4). Four models were derived based on the width of the slab that was being cast. These widths are 1060mm, 1280mm to 1290mm, 1320 to 1335mm and 1575mm wide slabs. (No specific variability was noticed when training the models using data which were divided based on the type of steel cast *e.g.* austenitic, ferritic, *etc.*). The normalised inputs used in the training of the 1060mm wide slab models are shown in Figs. 3.13, 3.14 and 3.15. Three important points for the regression procedure have to be mentioned here.

1. The value of the first point of the (time) data used is subtracted from all the data for each input variable so that the regression can be done with data starting from zero. The value of this first data point was then considered to be the offset of the data, and all data then become deviational from this point. This method delivered better results than simply removing the mean of the training data ("zero-order detrend").

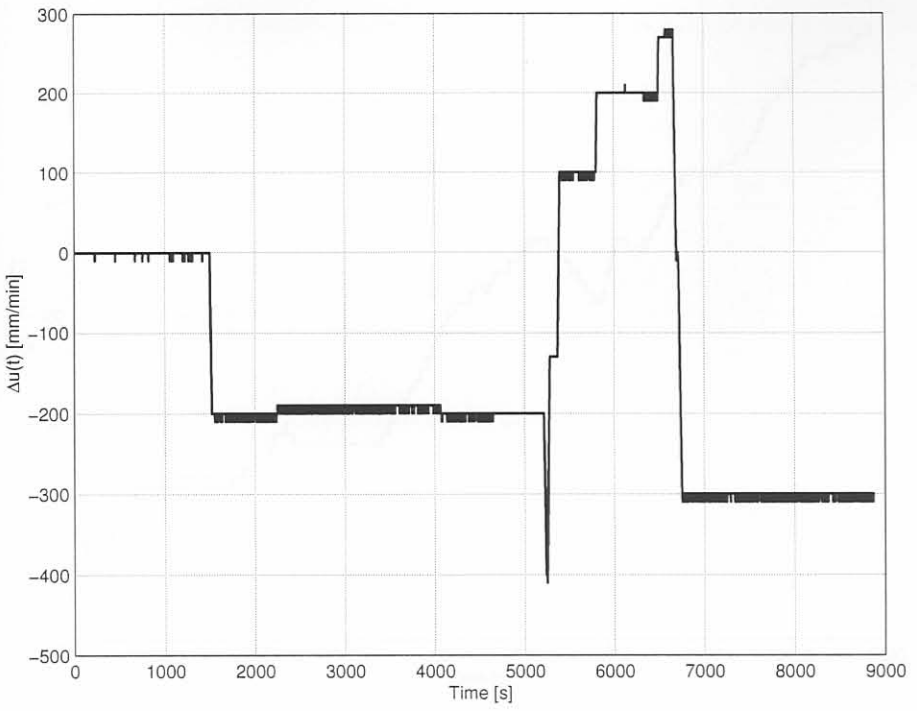

Figure 3.13 Casting speed input ($\Delta u(t)$) used for the training of the MVIV model for 1060mm wide slabs.

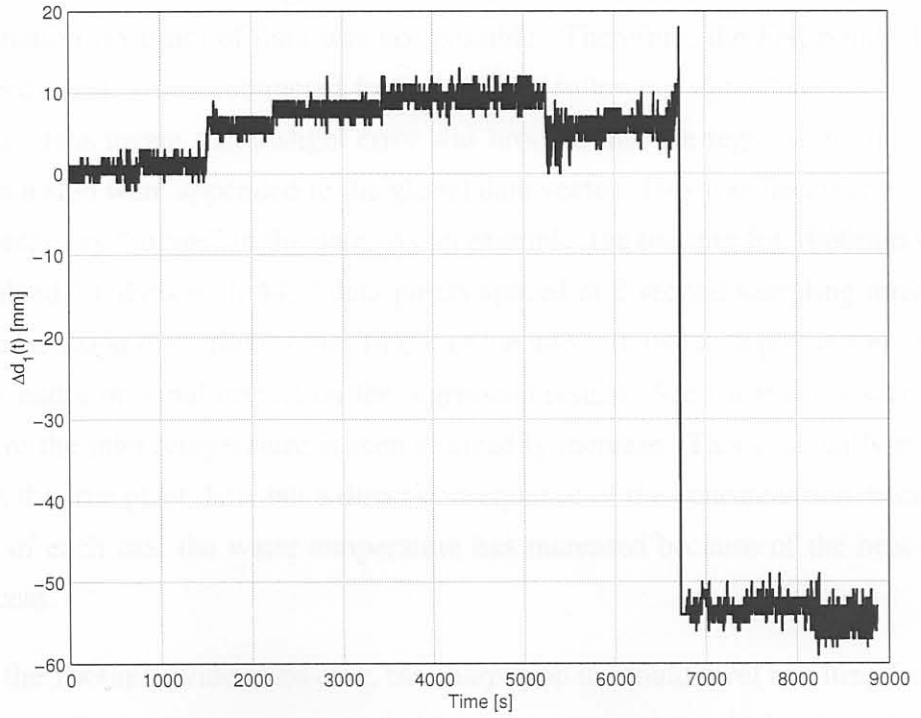

Figure 3.14 Mould level disturbance input ($\Delta d_1(t)$) used for the training of the MVIV model for 1060mm wide slabs.

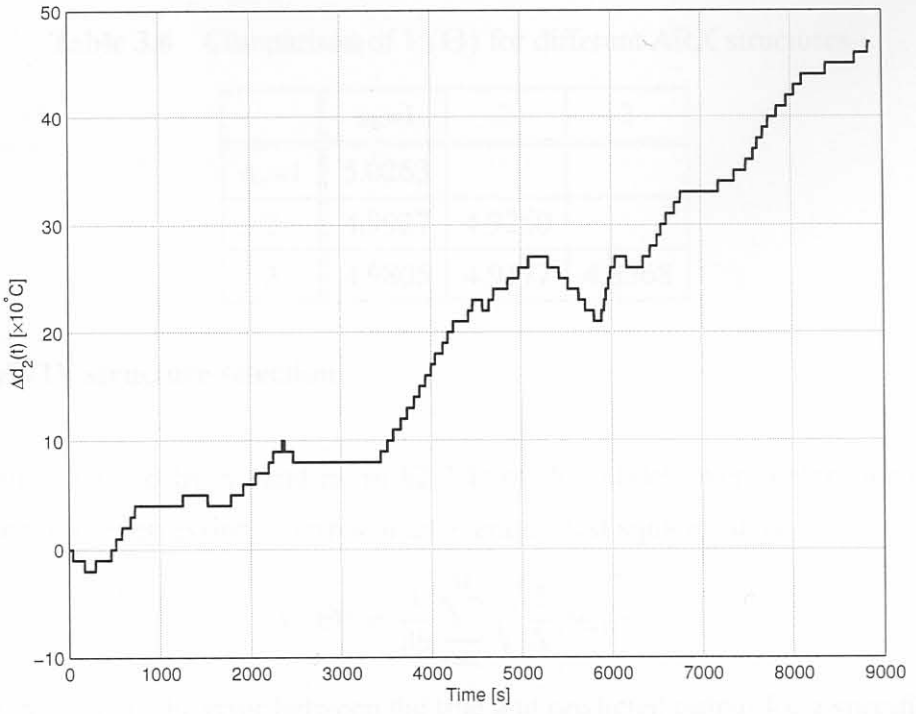

Figure 3.15 Water temperature disturbance input ($\Delta d_2(t)$) used for the training of the MVIV model for 1060mm wide slabs.

2. Since slabs that were inspected did not necessarily follow each other, simple concatenation (in time) of data was not possible. Therefore, the first point of data of a preceding slab was subtracted from data of a following slab. This was done for all slabs. This meant that a slight error was brought into the regression every time data from a slab were appended to the global data vector. This was necessary to eliminate unnecessary "jumps" in the data. As an example, the training for 1060mm wide slabs involved 14 slabs with 4437 data points spaced at 2 second sampling intervals. The concatenation then implies that 14 out of the 4437 (0.3%) data points were erroneous. This had a minimal impact on the regression results. See for interest sake Fig. 3.15 where the inlet temperature is seen to steadily increase. This is actually not the case with the true plant data, but a direct consequence of the concatenation, because at the end of each cast the water temperature has increased because of the heat extraction process.

3. For the 1060mm wide slabs case, the sharp drop in mould level resulting from a sharp decrease in casting speed, is probably due to manual mould level control. This is another reason to include mould level in the model.

Table 3.6 Comparison of $V(\hat{\Theta})$ for different ARX structures.

	n_b=1	2	3
n_a=1	5.0263		
2	4.9927	4.9260	
3	4.9805	4.9177	4.8368

3.3.1.2 MVIV structure selection

The structure (defined by n_a and n_b in §2.2.4) of the models were determined based on performance of the regression in terms of an average least squares fit as

$$V(\hat{\Theta}) = \frac{1}{38}\sum_{i=1}^{38}\sqrt{\frac{1}{N}||\epsilon_i||^2}, \tag{3.8}$$

where $\epsilon_i = \mathbf{y}_i - \hat{\mathbf{y}}_i$ is the error between the true and predicted output for a specific output i, over some time period, $t_0 \leq t \leq t_1$. $||\cdot||$ is the Euclidean norm. N is the number of data points used. The output matrices of Eq. 2.19 are all assumed to be diagonal, since none of the thermocouples are assumed to influence each other. As an example, consider the results of a regression on the 1060mm wide slabs as a function of n_a and n_b; depicted in Table 3.6. The table shows that an increase in regressors (model parameters) does not greatly improve the overall accuracy of the model. For instance, an increment in the number of poles from one to two (*i.e.* n_a increases from one to two while $n_b = 1$) only delivers a 0.7% increase in the overall fit. An increase from $n_a = 1$ and $n_b = 1$ to $n_a = 3$ and $n_b = 3$ only delivers an 3.8% decrease in the error[p]. This is further emphasised when looking at a plot of the model output for one thermocouple, in1u ($\Delta y_1(t)$), with $n_a = 1$ and $n_b = 1$ and $n_a = 3$ and $n_b = 3$ (Fig. 3.16). The figures show that the maximum change is about 2.5°C. Due to this close proximity of the models, the simple first order model ($n_a = 1$ and $n_b = 1$) was used to train the model. Similar results were obtained for the other outputs. Note that no visible delay is detected in the analysis of the residuals.

3.3.1.3 MVIV time domain results

Computer simulation of the model with plant inputs and outputs used to train the MV to IV model delivered good results. Fig. 3.17 shows the output of the model versus the true

[p]For 1280 mm wide slabs, the increase from $n_a = 1$ and $n_b = 1$ to $n_a = 3$ and $n_b = 1$ delivers a 1.2% improvement and for 1575mm wide slabs the increase from $n_a = 1$ and $n_b = 1$ to $n_a = 3$ and $n_b = 3$ delivers a 1.1% improvement. See Appendix D.

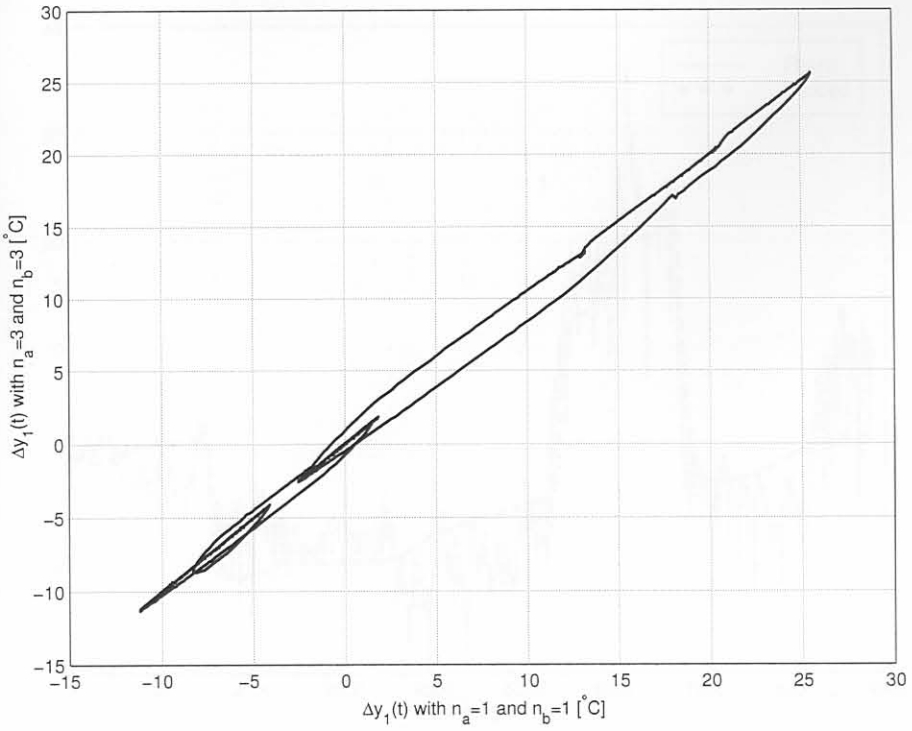

Figure 3.16 Comparison of model outputs for different structures of the MV to IV model for thermocouple in1u ($\Delta y_1(t)$).

plant data for thermocouple in1u (output $\Delta y_1(t)$) for 1060mm wide slabs. Similarly, Fig. 3.18 and Fig. 3.19 show the model and plant outputs for thermocouples nr1u ($\Delta y_{35}(t)$) and nr2u ($\Delta y_{37}(t)$) respectively. Note that similar results were found for 1280mm wide slabs and 1575mm wide slabs. See Appendix D. The noise that is visible can be attributed to measurement noise on the thermocouples; and also unmodelled dynamics because of unmeasured disturbances such as varying flux thickness layers at the mould-strand interface and other unmeasured disturbances such as superheat, steel flow rate *etc.*

3.3.1.4 Validation of the MVIV model

Two-thirds of the data were used to train the MVIV models and one third were used for validation of the MVIV model. Figs. 3.20 and 3.21 show the model outputs for thermocouples in2u and nr1u of the 1280mm wide model based on the *validation data* (not used for model fitting). The inputs (casting speed, mould level and water temperature) can be found in appendix E. The model output follows the true plant data reasonably accurately. The same can be said about the response of the other thermocouples as well as the response of the 1060mm and 1575mm wide slab validation data.

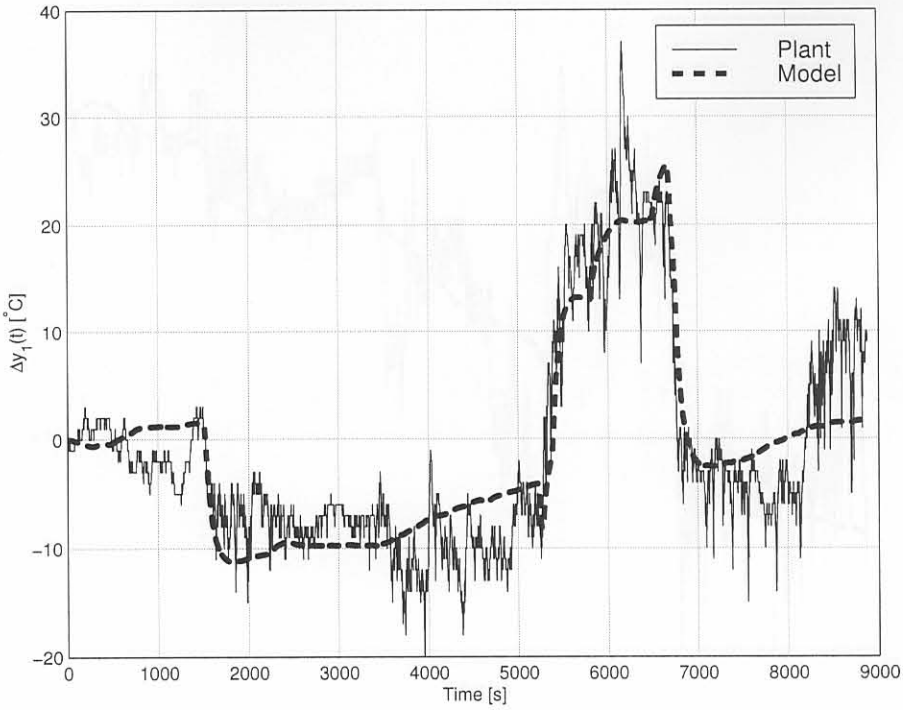

Figure 3.17 Comparison of model output and plant output for thermocouple (output) in1u ($\Delta y_1(t)$) with $n_a = 1$ and $n_b = 1$. The mean square fit is $\sqrt{||\epsilon_1||^2/N} = 4.341$.

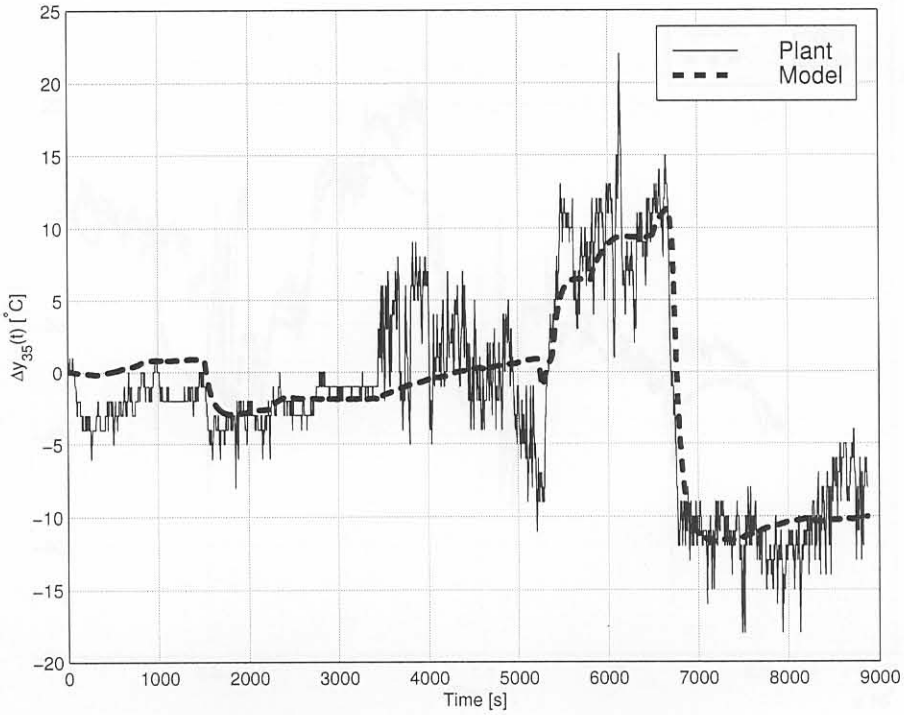

Figure 3.18 Comparison of model output and plant output for thermocouple (output) nr1u ($\Delta y_{35}(t)$) with $n_a = 1$ and $n_b = 1$. $\sqrt{||\epsilon_{35}||^2/N} = 3.131$.

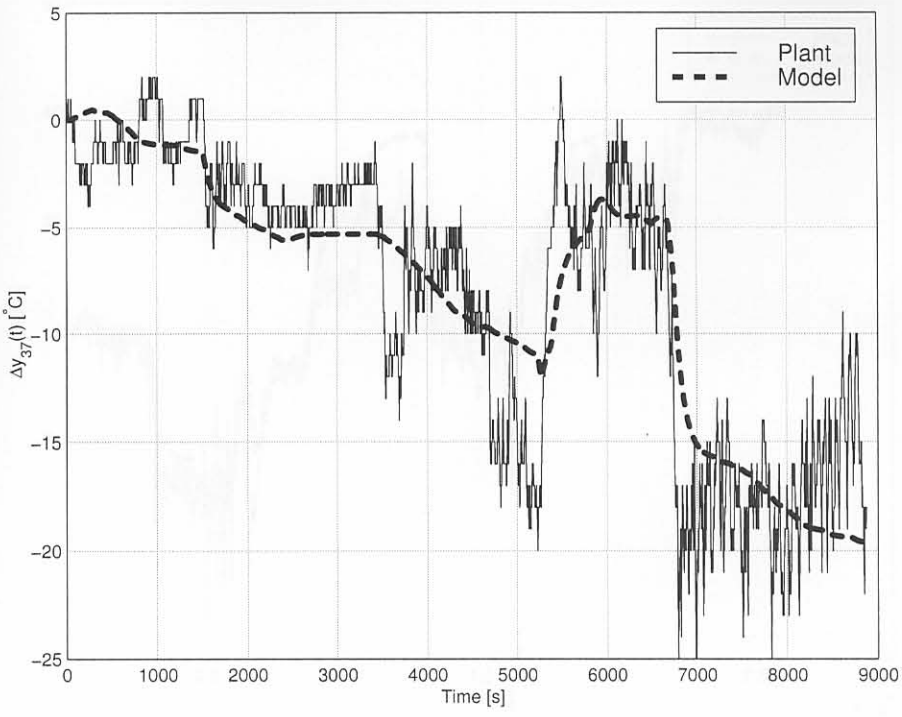

Figure 3.19 Comparison of model output and plant output for thermocouple (output) nr2u ($\Delta y_{37}(t)$) with $n_a = 1$ and $n_b = 1$. $\sqrt{||\epsilon_{37}||^2/N} = 3.235$.

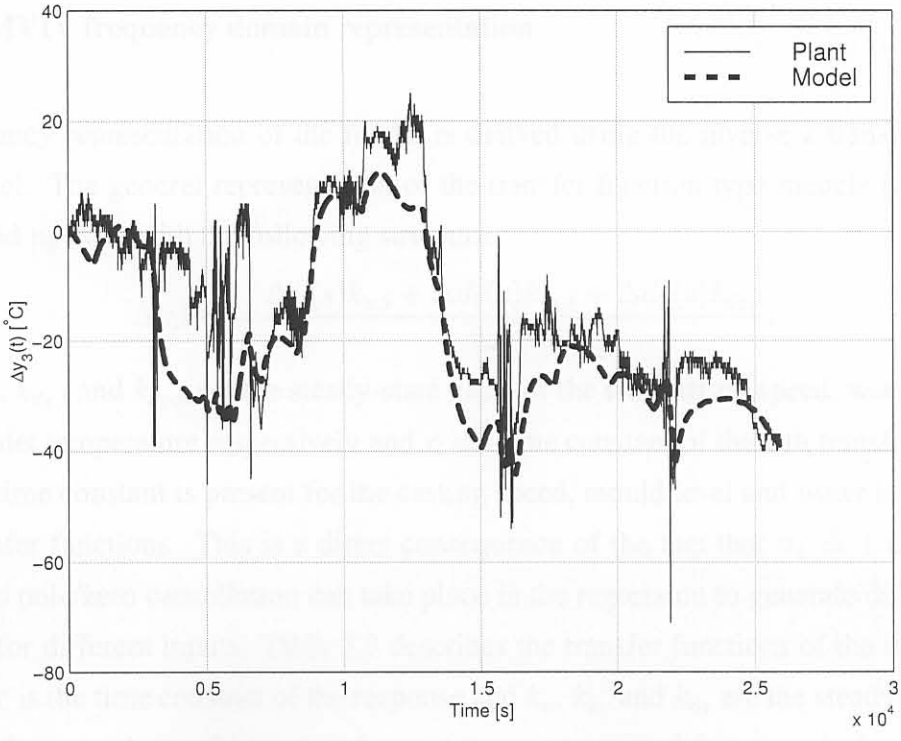

Figure 3.20 Comparison of model output and plant output for thermocouple (output) in2u ($\Delta y_3(t)$) on the *validation data* for 1280mm wide slabs. $\sqrt{||\epsilon_3||^2/N} = 10.411$

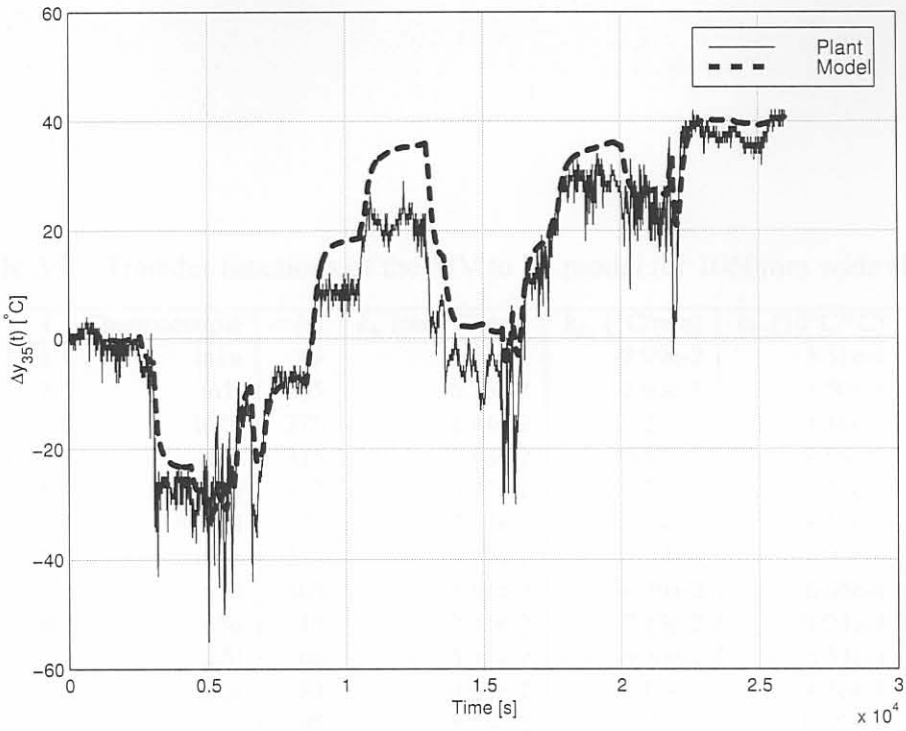

Figure 3.21 Comparison of model output and plant output for thermocouple (output) nr1u ($\Delta y_{35}(t)$) on the *validation data* for 1280mm wide slabs. $\sqrt{||\epsilon_{35}||^2/N} = 7.670$

3.3.1.5 MVIV frequency domain representation

The frequency representation of the model is derived using the inverse z-transform of the ARX model. The general representation of the transfer function type models is first order ($n_a = 1$ and $n_b = 1$) with the following structure.

$$\Delta y_i(s) = \frac{\Delta u(s)k_{u,i} + \Delta d_1(s)k_{d_1,i} + \Delta d_2(s)k_{d_2,i}}{\tau_i s + 1}, \tag{3.9}$$

where $k_{u,i}$, $k_{d_1,i}$ and $k_{d_2,i}$ are the steady-state gains of the i-th casting speed, water temperature and inlet temperature respectively and τ_i the time constant of the i-th transfer function. Only one time constant is present for the casting speed, mould level and water inlet temperature transfer functions. This is a direct consequence of the fact that $n_a = 1$ and $n_b = 1$ because no pole/zero cancellation can take place in the regression to generate different time constants for different inputs. Table 3.7 describes the transfer functions of the model. In the table, τ is the time constant of the response and k_u, k_{d_1} and k_{d_2} are the steady-state gains of the casting speed, mould level and water temperature models respectively. The time-constants vary greatly from values as low as 17 seconds (in5u) to as high as 606 seconds (ou7l). This can be attributed to several factors. Firstly, the contact of the thermocouple to the copper plate may vary from thermocouple to thermocouple, thus making the thermal

Table 3.7 Transfer functions of the MV to IV model for 1060mm wide slabs.

i	Thermocouple	τ [s]	k_u [min°C/mm]	k_{d_1} [°C/mm]	k_{d_2}[10°C/°C]
1	in1u	69	6.07e-2	-8.99e-2	3.31e-1
2	in1l	185	6.75e-2	-2.93e-1	7.50e-1
3	in2u	276	1.44e-2	9.27e-2	-4.16e-1
4	in2l	315	1.88e-2	-9.87e-2	-4.64e-1
5	in3u	117	4.07e-2	1.21e-2	1.58e-1
6	in3l	221	3.22e-2	-1.94e-1	-8.18e-2
7	in4u	235	3.94e-2	1.19e-1	7.96e-1
8	in4l	305	5.51e-2	-6.39e-2	6.05e-1
9	in5u	17	3.11e-2	7.13e-2	1.21e-1
10	in5l	206	5.11e-2	-9.30e-2	5.51e-1
11	in6u	84	4.69e-2	-8.80e-2	4.10e-1
12	in6l	298	8.24e-2	-2.92e-1	1.35e+0
13	in7u	127	4.33e-2	-7.68e-2	2.75e-1
14	in7l	226	6.33e-2	-9.39e-2	9.24e-1
15	in8u	72	3.99e-2	-2.63e-2	1.22e-1
16	in8l	135	4.57e-2	1.41e-1	7.22e-1
17	nl1u	62	1.78e-2	-2.31e-2	1.12e-1
18	nl1l	87	1.34e-2	-1.27e-1	-4.22e-3
19	nl2u	122	1.72e-2	1.90e-1	-3.13e-2
20	nl2l	117	2.44e-2	-4.24e-2	-4.49e-1
21	ou1u	101	6.44e-2	-2.00e-1	-2.48e-2
22	ou1l	165	5.92e-2	5.35e-2	6.43e-1
23	ou2u	137	6.42e-2	-1.40e-1	2.92e-1
24	ou2l	210	6.89e-2	-1.72e-1	5.85e-1
25	ou3u	235	3.49e-2	-1.24e-1	-5.65e-1
26	ou3l	324	6.06e-2	-2.39e-1	-1.74e-1
27	ou4u	241	3.04e-2	3.40e-2	-1.58e-1
28	ou4l	434	2.41e-2	3.17e-2	-3.93e-1
29	ou5u	136	3.82e-2	-2.17e-2	5.15e-1
30	ou5l	247	6.41e-2	-6.37e-2	9.66e-1
31	ou7u	228	7.08e-2	-7.64e-3	1.09e+0
32	ou7l	606	9.65e-2	6.27e-2	2.54e+0
33	ou8u	66	6.82e-2	-2.03e-1	1.70e-1
34	ou8l	169	7.56e-2	-1.70e-1	1.12e+0
35	nr1u	69	2.28e-2	1.77e-1	1.41e-1
36	nr1l	108	2.34e-2	1.16e-1	4.94e-1
37	nr2u	100	1.60e-2	2.02e-2	-2.99e-1
38	nr2l	120	8.71e-3	-2.99e-2	-1.42e-1

resistance different, causing a longer time constant. The effect that an increase in the air gap between the copper and thermocouple has on the thermal resistance (proportional to time constant) is shown in fig. 3.22.

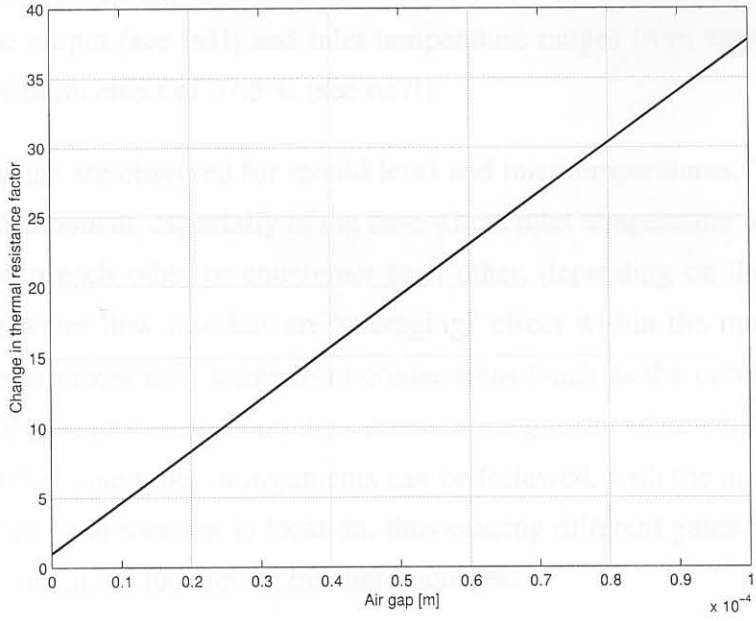

Figure 3.22 Proportional increase in the time constant of the temperature measured by a thermocouple.

The graph was calculated using a convection model describing the proportional change in thermal conductivity of the system when the air gap increases compared to the case when there is no air gap [165]:

$$R_{ch} = \frac{l_{air}/k_{air}}{l_{copper}/k_{copper} + l_{typeK}/k_{typeK}} + 1, \tag{3.10}$$

where l_{air} is the air gap, $l_{copper} = 35$mm is the copper-plate width, $l_{typeK} = 1$mm is the casing width of the thermocouple, and $k_{copper} = 386$W/mK, $k_{air} = 0.027$W/mK, and $k_{typeK} = 65$W/mK are the respective thermal conductivities. An air gap of 90μm caused by a shock to the mould during installation can cause the time constant to increase by a factor of 35 (*e.g.* from 17 to 600 seconds). Good thermocouple installation and maintenance is therefore very important if correct readings are desired. Secondly, the mould plate may vary in thickness from area to area, thus making the thermal resistance different. Thirdly, there may be more mould flux situated in different areas, making the thermal resistance different.

The time constants also increase from the top row to the bottom row, indicating that an increasing shell thickness causes a greater thermal resistance.

Though not immediately clear, the casting speed has the greatest steady-state effect on the outputs. This is because the casting speed can range from 0 to 1000 mm/min. A change of 1000mm/min can have a maximum effect of a 96.5°C change on the ou7l output[q] at steady state. Similarly, mould level ranges from about 0 to 60mm and can have a maximum effect of 17.6°C on the output (see in1l) and inlet temperature ranges from approximately 25 to 40°C with a maximum effect of 37.5°C (see ou7l).

Some negative gains are observed for mould level and inlet temperatures. This may be due to a non-linear component, especially in the case where inlet temperature and casting speed either interact with each other or counteract each other, depending on the temperature of the strand. The water flow also has an "averaging" effect within the mould, since water from warmer areas mixes with water from colder areas (such as the corners), thus having the possibility of a negative effect on the output (see *e.g.* nl1l, nl2u, nl2l, nr2u and nr2l). For mould level the same types of arguments can be followed, with the most feasible being that the flux varies from location to location, thus causing different gains depending on the thickness of the flux at the location of the thermocouple.

Many other (unmeasured) disturbances are also present which can play a role in determining the model parameters. The ARX scheme used is simple to understand and to train and is useful for control system analysis and design. It also proves adequate as a modelling scheme for the MVIV model, in both the frequency and time domains.

See the frequency domain tables in Appendix F for 1280mm and 1575mm wide slabs.

Figs. 3.23, 3.24 and 3.25 depict Bode plots between casting speed, mould level and inlet temperature and the thermocouple temperatures, respectively. Appendix F show the frequency responses for 1280mm and 1575mm wide slabs.

This section presented the MV to IV model derivation using ARX techniques. The resulting model to plant fits are considered very good as shown by the training and validation data, given that there are unmeasured disturbances interacting on the system. Not all data can be shown, due to constraints of space. The MV to IV model can be used to design controllers to follow pre-defined set-points for the thermocouple temperatures.

[q] ou7l has the largest steady state gain

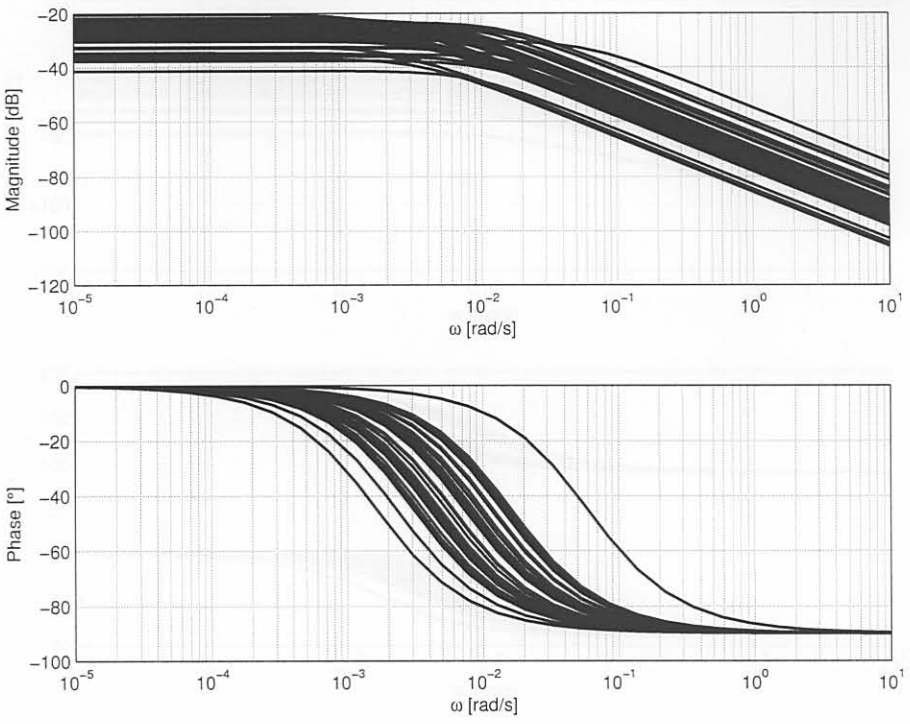

Figure 3.23 Bode plot of the transfer functions between casting speed and the thermocouple temperatures for 1060mm wide slabs.

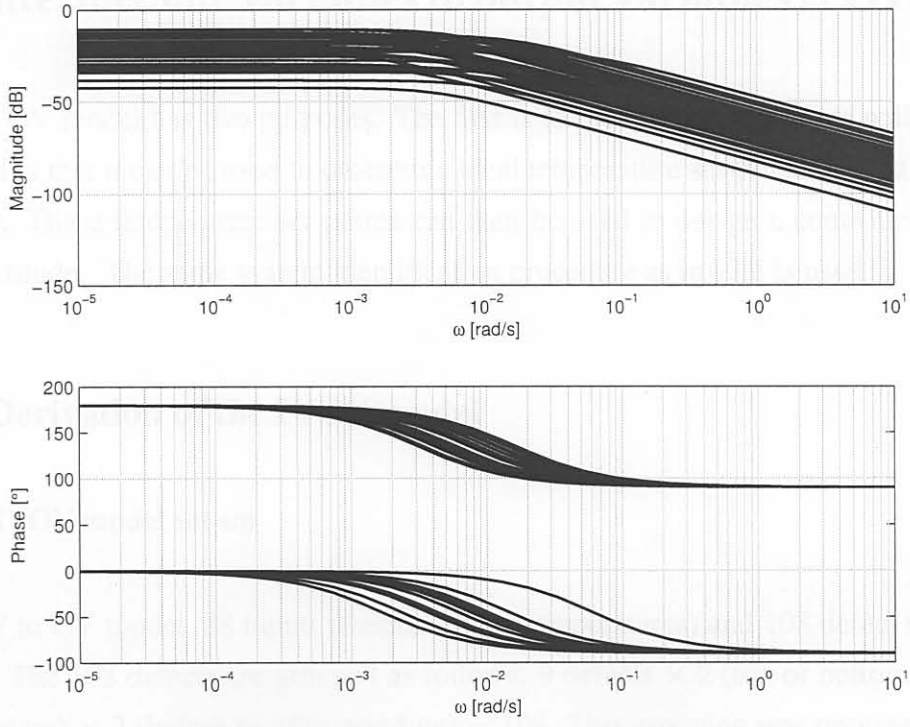

Figure 3.24 Bode plot of the transfer functions between mould level and the thermocouple temperatures for 1060mm wide slabs.

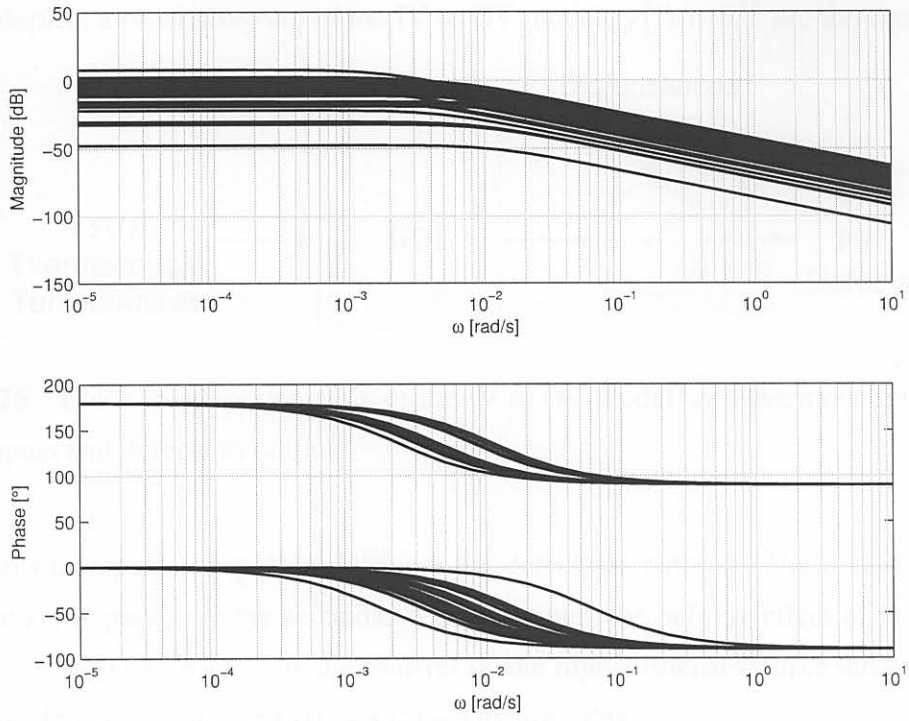

Figure 3.25 Bode plot of the transfer functions between inlet temperature and the thermocouple temperatures for 1060mm wide slabs.

3.4 Intermediate variables to output variables (IVOV) model

The IV to OV model has two purposes. The first is to predict when a defect will occur and the second is that it can be used to determine ideal temperature set-points so that no defects will occur. These temperature set-points can then be used to design a controller using the MV to IV model. The same system identification procedure as in §3.3 is used.

3.4.1 Derivation of the IVOV model

3.4.1.1 IVOV model set-up

For the IV to OV model, 38 inputs (thermocouple temperatures) and 108 defect outputs are available. The 108 defects are grouped as follows: 9 defects $\times$ 2 (top or bottom) $\times$ 3 (left, right or centre) $\times$ 2 (before or after grinding) $= 108$. This grouping was necessary because the defects roughly correspond to the location of the thermocouples. Therefore $m = 38$ and $p = 108$.

Fig. 3.26 depicts a block diagram of the IV to OV model. $\mathbf{y}(t) \in \mathbb{R}^{38}$ are the thermocouple

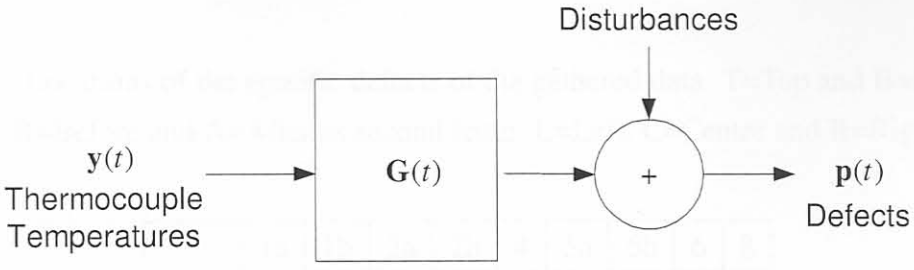

Figure 3.26 Block diagram depiction of the IV to OV model with thermocouple temperatures as inputs and defects as outputs.

temperatures as inputs and $\mathbf{p}(t) \in \mathbb{R}^{108}$ are the defects as outputs. The disturbances may include the spray pattern in the secondary cooling zone[r], the bulging effect of the rollers on the strand *etc.* $\mathbf{G}(t) \in \mathbb{R}^{108\times 38}$ is the transfer of the inputs (thermocouple temperatures) to the outputs (defects) in $\mathbf{p}(t) = \mathbf{G}(t) * \mathbf{y}(t) + \text{Disturbances}$.

Though 108 defects can theoretically be expected, only 70 defects actually occurred during the data gathering period. The defects that did occur are indicated with a • in Table 3.8. Naturally, if defects do not occur, they cannot be detected in the regression and hence do not form part of the model. However, because the structure can later be extended to included defects at all locations, it will be assumed that there are 108 defects present for the model structure definition.

3.4.1.2 IVOV structure selection

The same procedure was followed as with the MVIV model to determine the structure of the model. Table 3.9 shows the mean least squares (as an example) for the longitudinal crack defect (which shows up on the top left portion of the slab only after grinding) with different values for n_a and n_b. A more accurate fit was obtained as the structure size was increased. Based on this result and the fits of the other defects, the optimal choice for the structure was $n_a = 5$ and $n_b = 4$. This model structure contains enough information to detect the defects, and is not too large to handle during training and simulation[s].

Note that no real difference could be detected between the types of steels cast and the widths

[r] see *e.g.* Barozzi, Fontana, and Pragliola [166]

[s] Training was done on a 256MB RAM, 1GHz PentiumIII machine, with typical training times of about 30 minutes.

Table 3.8 Locations of the specific defects of the gathered data. T=Top and B=Bottom as first letter. B=Before and A=After as second letter. L=Left, C=Centre and R=Right as third letter.

	1a	1b	2a	2b	4	5a	5b	6	8
TBL			•	•	•	•	•	•	•
TBC			•	•	•	•	•	•	•
TBR			•	•	•	•	•	•	•
BBL				•		•	•	•	•
BBC				•		•	•	•	•
BBR				•		•	•	•	•
TAL	•			•		•	•	•	•
TAC	•	•		•		•	•	•	•
TAR				•		•	•	•	•
BAL				•		•	•	•	•
BAC			•	•		•	•	•	•
BAR				•		•	•	•	•

Table 3.9 Comparison of $V(\hat{\Theta})$ for different ARX structures for the IVOV model for longitudinal cracks.

	n_b=1	2	3	4	5	6
n_a=1	0.4663					
2	0.4462	0.4583				
3	0.4344	0.4458	0.4314			
4	0.4276	0.4427	0.4285	0.4210		
5	0.4245	0.4418	0.4276	0.4200	0.4166	
6	0.4228	0.4421	0.4275	0.4197	0.4160	0.4143

of the slabs that were cast. Therefore, only one model was derived including all widths and types of steel. The model was, however, derived for each specific defect, to lessen the burden on the processing machine (see footnote s). Data of slabs which have a specific defect and data of slabs with similar characteristics (*i.e.* widths and types) but without defects were included in the training set. This was to ensure that the model also has data where no defects occur to train with.

3.4.1.3 IVOV time domain results

The training procedure of the IVOV model gave satisfactory results on the training data with the structure defined above. Fig. 3.27 shows the model vs. plant output for a transversal crack occurring on the top left location after grinding has taken place. Though the estimate

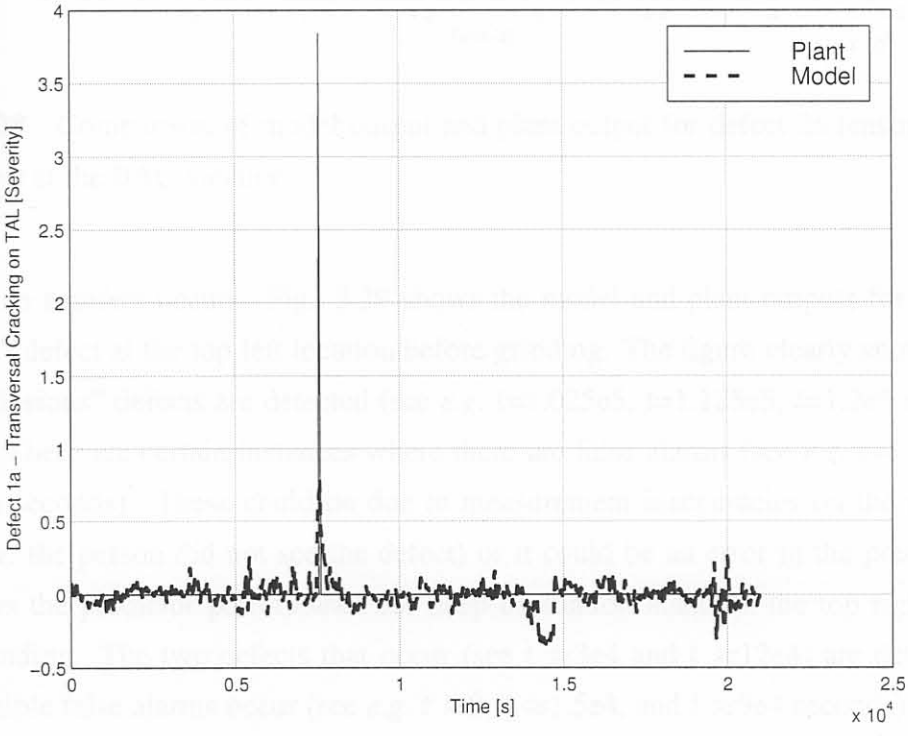

Figure 3.27 Comparison of model output and plant output for defect 1a (transversal crack) at the TAL location.

does not follow the defect output perfectly, a clear increase in the model output is observed when a defect occurs. This non-perfect following is probably due to the fact that the defect measurements are taken by humans and that the severity scale is probably not ordinal. Fig. 3.28 shows the model and plant output for casting powder entrapment at the bottom centre location after grinding. This result is also adequate with a substantial increase in the model

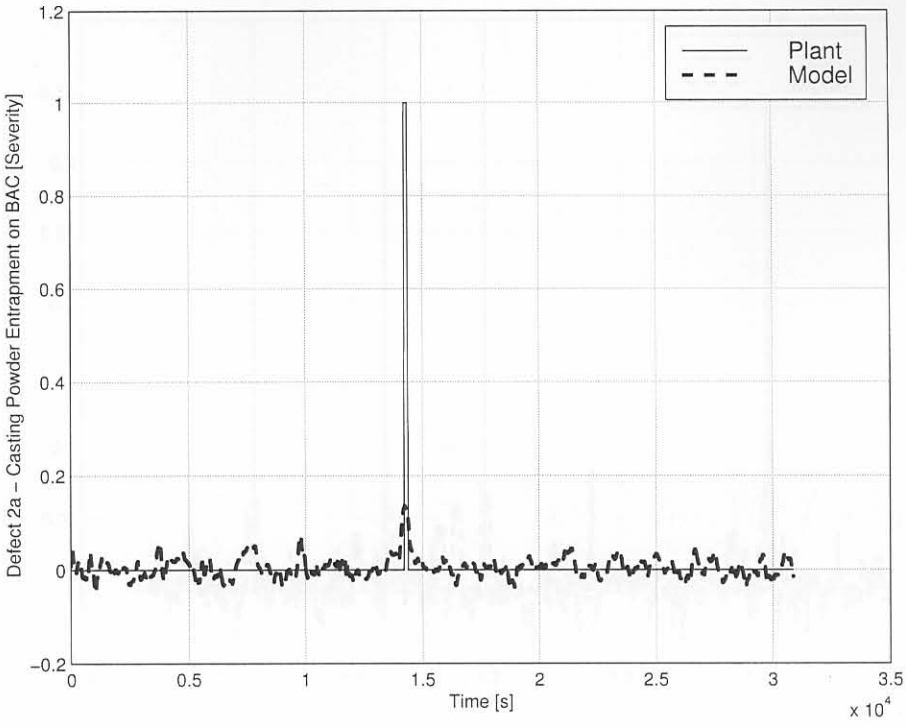

Figure 3.28 Comparison of model output and plant output for defect 2a (casting powder entrapment) at the BAC location.

output when a defect occurs. Fig. 3.29 shows the model and plant outputs for the "other inclusions" defect at the top left location before grinding. The figure clearly shows that the "other inclusions" defects are detected (see *e.g.* t=1.025e5, t=1.125e5, t=1.2e5 and 1.42e5 seconds). There are certain instances where there are false alarms (see *e.g.* t=1.175e5 and t=1.275e5 seconds). These could be due to measurement inaccuracies on the part of the human (*i.e.* the person did not see the defect) or it could be an error in the predictor. Fig 3.30 shows the predictor performance for deep oscillation marks at the top right position before grinding. The two defects that occur (see t ≈3e4 and t ≈12e4) are detected, and some possible false alarms occur (see *e.g.* t ≈0, t ≈1.5e4, and t ≈9e4 seconds). Fig. 3.31 shows the model output for stopmarks at the bottom centre location before grinding. Fig. 3.32 shows the predictor output for depressions at the top left location before grinding has taken place.

The predictor performance using validation data will be discussed in §3.4.5.

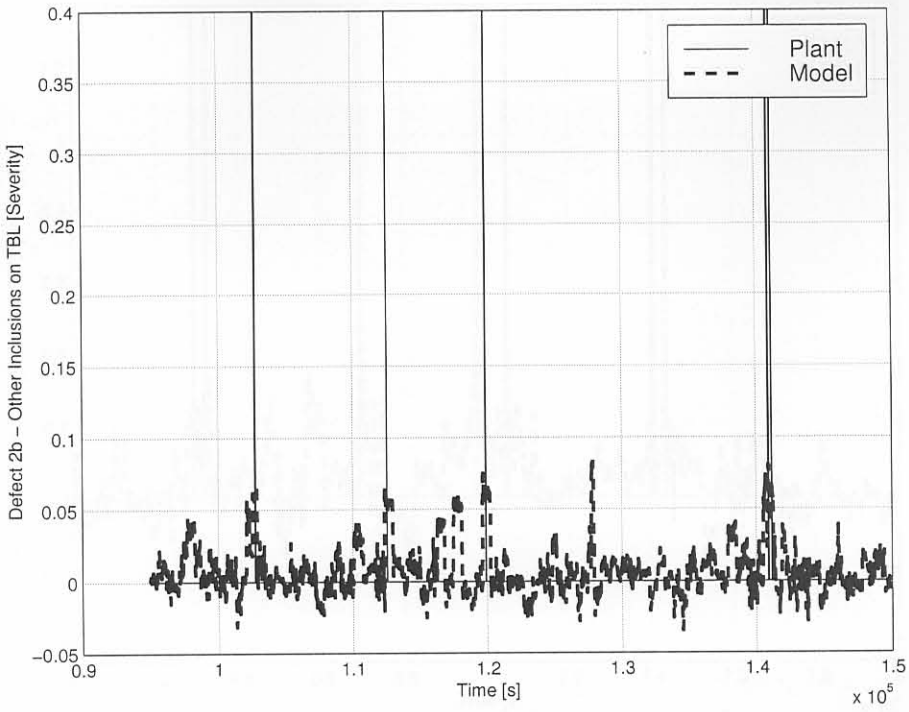

Figure 3.29 Comparison of a portion of the model output and plant output for defect 2b (other inclusions) at the TBL location.

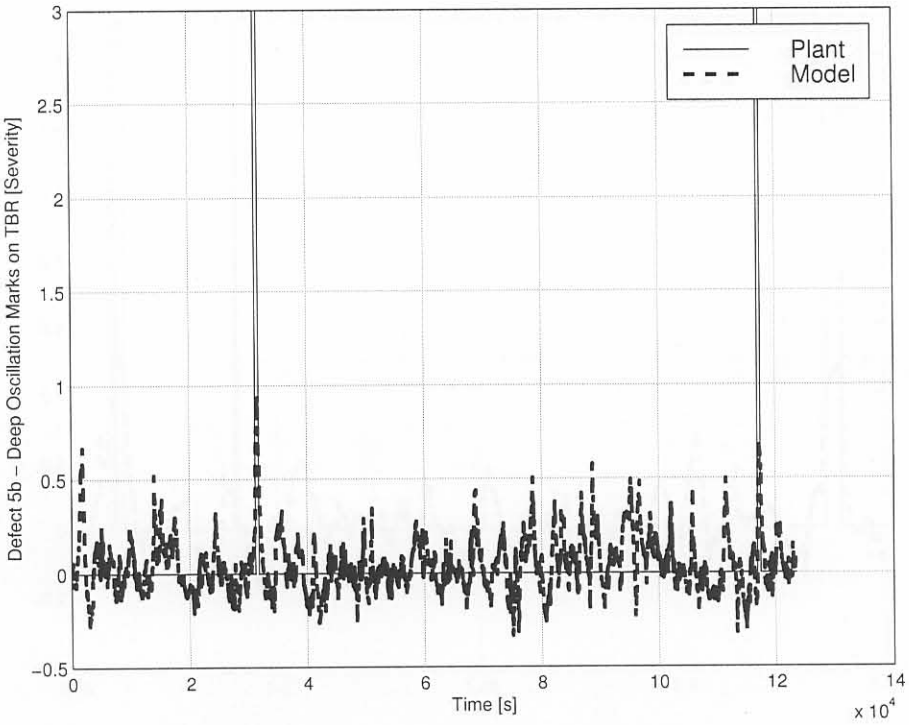

Figure 3.30 Comparison of the model output and plant output for defect 5b (deep oscillation marks) at the TBR location.

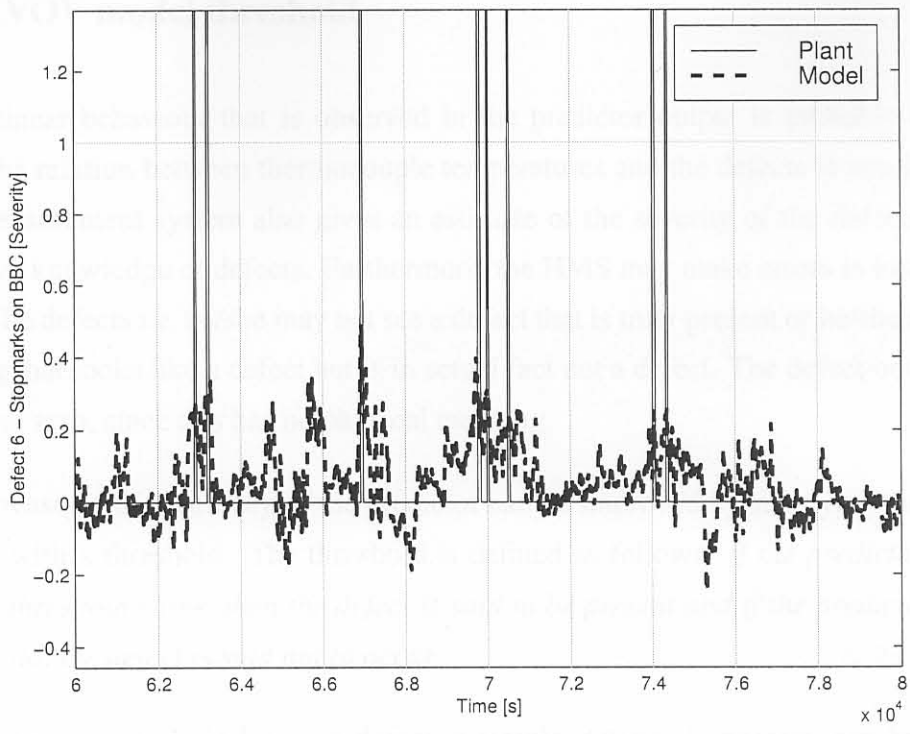

Figure 3.31 Comparison of a portion of the model output and plant output for defect 6 (stopmarks) at the BBC location.

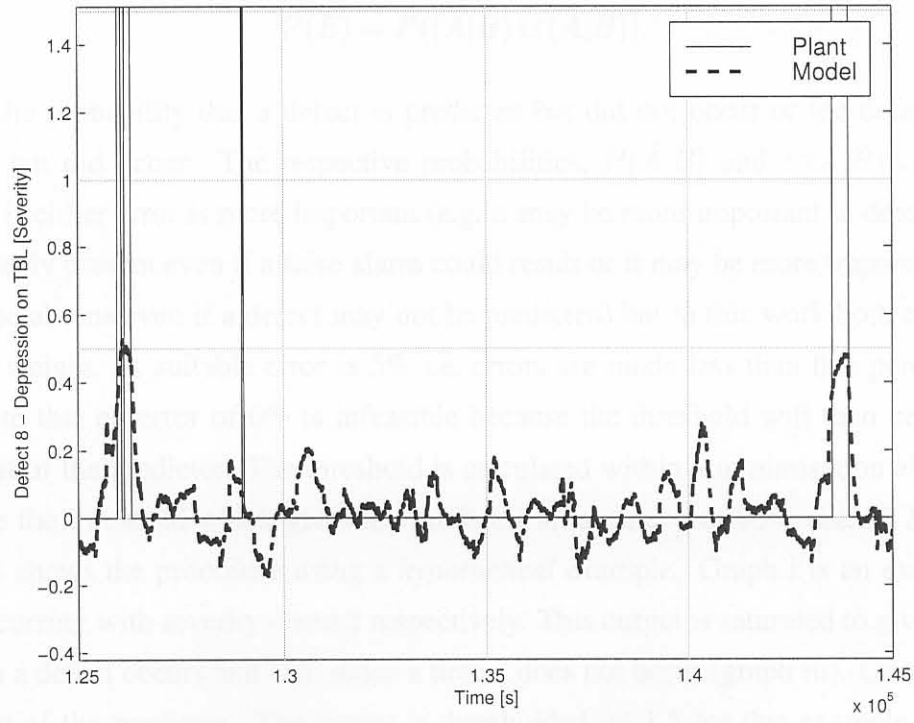

Figure 3.32 Comparison of a portion of the model output and plant output for defect 8 (depression) at the TBL location.

3.4.2 IVOV model threshold

The non-linear behaviour that is observed in the predictor output is probably due to the fact that the relation between thermocouple temperatures and the defects is non-linear. The human measurement system also gives an estimate of the severity of the defects based on his/her own knowledge of defects. Furthermore, the HMS may make errors in his/her observation of the defects *i.e.* he/she may not see a defect that is truly present or he/she may notice something that looks like a defect but is in actual fact not a defect. The defect output cannot be less than zero, since this has no physical meaning.

For these reasons, the accuracy of the predictor can be improved by supplying the detection algorithm with a threshold. The threshold is defined as follows: *if the predictor output is above the threshold value, then the defect is said to be present and if the predictor is below the threshold, the defect is said not to occur.*

To determine the threshold for each defect, a simple statistical approach can be followed. Define A as the event that a defect occurs over time and B as the event that a defect is predicted. Then $\bar{A}$ is the event that a defect does not occur and $\bar{B}$ is the event that a defect was not predicted. Then the probability of a prediction error occurring is given by

$$P(E) = P((\bar{A}|B) \cup (A|\bar{B})). \tag{3.11}$$

$P(E)$ is the probability that a defect is predicted but did not occur or the defect was not predicted but did occur. The respective probabilities, $P(\bar{A}|B)$ and $P(A|\bar{B})$ can also be weighted if either error is more important (*e.g.* it may be more important to detect a defect which is truly present even if a false alarm could result or it may be more important to have fewer false alarms even if a defect may not be predicted) but in this work both errors carry the same weight. A suitable error is 5% *i.e.* errors are made less than five percent of the time. Note that an error of 0% is infeasible because the threshold will then be set above any output of the predictor. The threshold is calculated within a minimisation algorithm to determine the threshold which gives the predictor an accuracy of 95% (*i.e.* $P(E) = 5\%$). Fig. 3.33 shows the procedure using a *hypothetical* example. Graph i is an example of a defect occurring with severity 4 and 2 respectively. This output is saturated to give values of one when a defect occurs and zero when a defect does not occur (graph iii). Graph ii shows the output of the predictor. The output is thresholded (at 1.5 for this example, see graph iv), and set to one to denote a predicted defect and zero to denote no predicted defect. The thresholded output of the predictor is then subtracted from the saturated plant output (graph v) and the absolute value of that difference is then used to predict $P(E)$ (graph vi). The

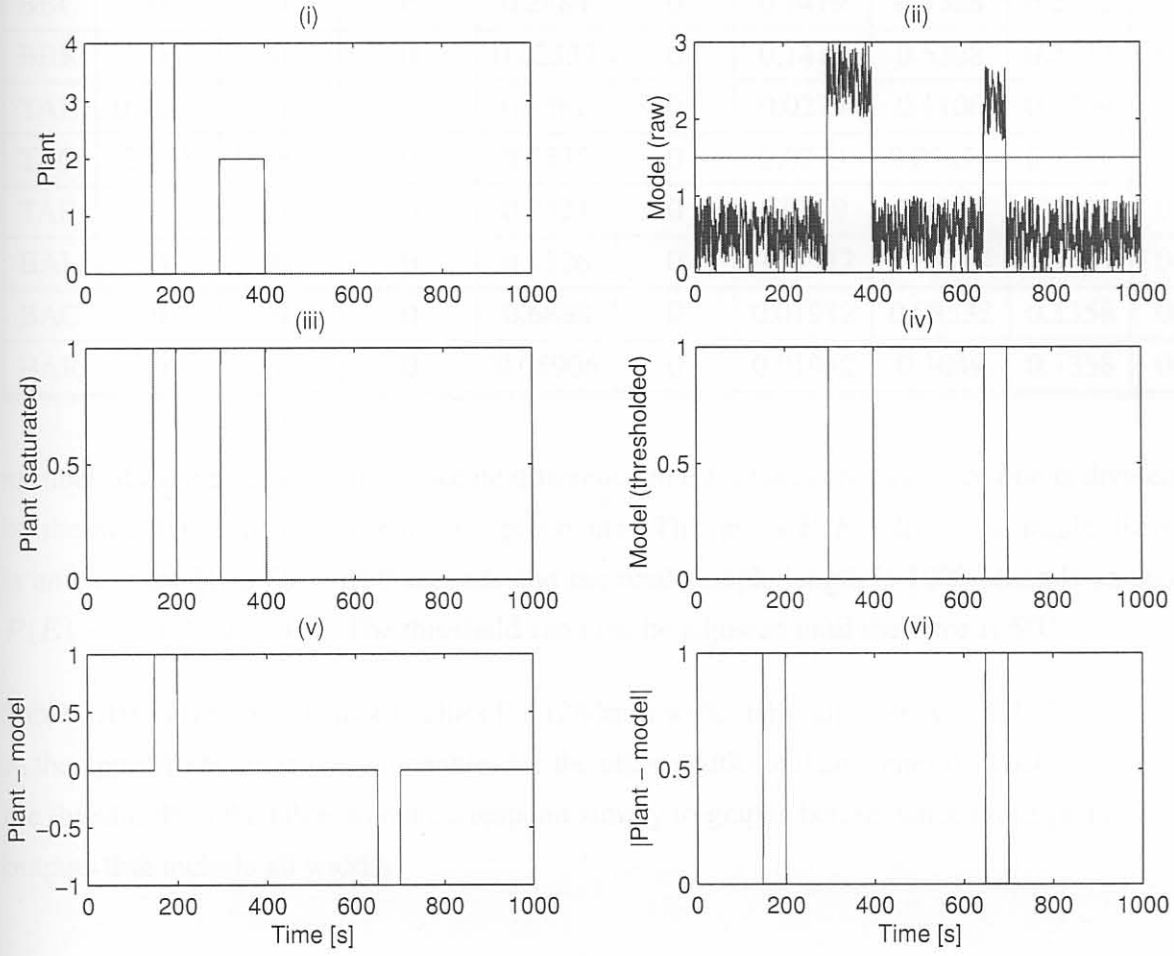

Figure 3.33 Procedure for the calculation of the accuracy of the thresholded predictor output.

Table 3.10 Thresholds for the IVOV predictor for 1280mm wide slabs

	1a	1b	2a	2b	4	5a	5b	6	8
TBL	0	0	0.07379	0.04115	0.4916	0.2216	0.5328	0.3374	0.1682
TBC	0	0	2.662	0.1922	0.1986	0.2187	0.5328	0.3374	0.08673
TBR	0	0	0.03544	0.0253	0.1632	0.1777	0.5328	0.3374	0.1826
BBL	0	0	0	0.06602	0	0.1419	0.5328	0.2732	0.1184
BBC	0	0	0	0.2484	0	0.1419	0.5328	0.2732	0
BBR	0	0	0	0.02357	0	0.1419	0.5328	0.2732	0.1485
TAL	0.7519	0	0	0.2362	0	0.0279	0.1106	0.1799	0.2018
TAC	2.155	0.5597	0	0.7575	0	0.0279	0.09825	0.1799	0.1946
TAR	0	0	0	0.2424	0	0.0279	0.1287	0.1799	0.2001
BAL	0	0	0	0.1126	0	0.01912	0.08764	0.1321	0.1556
BAC	0	0	0	0.6838	0	0.01912	0.08532	0.1358	0.2163
BAR	0	0	0	0.05906	0	0.01912	0.1049	0.1358	0.1455

number of time points that the absolute difference in error takes on a value of one is divided by the number of samples for the test procedure. This gives $P(E)$. In this example, there is an error for $50 + 50 = 100$ seconds and the total sample length is 1000 seconds so that $P(E) = 100/1000 = 0.1$. The threshold can now be adjusted until the error is 5%[t].

Table 3.10 shows the threshold values for 1280mm wide slabs; and tables G.1, G.2, and G.3 in the appendixes show the same tables for the other widths that are generally cast. Note that the thresholds in the table do not correspond simply to graphs before, since those graphs are outputs that include all widths.

3.4.3 IVOV model defected slabs ratios

A comparison of the number of defected slabs that should be sent for direct rolling, and the number of slabs that were predicted to have defects after the threshold has been applied is also informative. Table 3.11 shows the number of slabs that would have been *falsely* sent for grinding based on the output of the predictor for each defect and defect location. N is the number of slabs that were used in the training of the IVOV model. These values are somewhat conservative, since they are linked to a specific defect and location so that

[t]note that in this example it will not be possible to reach 5% since the predictor did not closely predict the defect at 150 seconds

Table 3.11 Number of slabs that would have been sent for processing based on a false alarm from the predictor per defect location using the training data.

	1a	1b	2a	2b	4	5a	5b	6	8
N	55	72	56	412	154	327	244	175	406
TBL	-	-	9	28	2	10	3	27	38
TBC	-	-	0	53	0	7	3	27	61
TBR	-	-	7	50	0	21	3	27	36
BBL	-	-	-	58	-	3	3	38	81
BBC	-	-	-	55	-	3	3	38	22
BBR	-	-	-	50	-	3	3	38	74
TAL	0	-	-	74	-	45	26	48	94
TAC	0	4	-	31	-	45	10	48	58
TAR	-	-	-	76	-	45	24	48	80
BAL	-	-	-	126	-	28	1	59	74
BAC	-	-	0	42	-	28	3	59	67
BAR	-	-	-	171	-	28	3	59	75
AV%	0.0	5.6	7.1	16.5	0.4	6.8	2.9	24.6	15.6

repetition could have occurred because the same slab may have been sent for grinding based on the outcome of the predictor for two or more defects or defect locations. For transversal cracks (1a), the ratio of false alarm slabs to cast slabs (N) is 0% . For longitudinal cracks (1b) it is 5.6% , and for casting powder entrapment it has a mean value of 7.1% [u]. One of the worst performing defects is other inclusions (2a) with a ratio of 16.5% , *i.e.* the conservative estimate of slabs with inclusions that should not have been sent for processing is 16.5% . For bleeders the figure is 0.43% and for deep oscillation marks (5a) it is, on average, 6.8% . For uneven oscillation marks (5b) the ratio is 2.9% , noting that the number of false alarms increases for predictions below surface (after grinding on the top of the slabs). For stopmarks the average value for the ratio is 24.6% and for depressions it is 15.6% .

Table 3.12 shows the ratio of slabs that were predicted to have a specific defect at a specific location to the number of slabs that did have the defect present. Note that these values are conservative because a slab that was not predicted to be defective on one defect and defect location may have been predicted to be defective based on another defect or defect location. Slabs with transversal cracks were identified perfectly, while longitudinal cracks has an accuracy of 33% . Casting powder entrapments were predicted perfectly while other inclusions

[u] AV% denotes the average ratio of falsely predicted slabs to total slabs over all locations.

Table 3.12 Number of slabs that should have been sent for processing based on the predictor where a slab was truly defected using the training data. In $x|y$, x is the number of slabs predicted to have the defect and y is the number of slabs that did have the defect present.

	1a	1b	2a	2b	4	5a	5b	6	8
N	55	72	56	412	154	327	244	175	406
TBL	-	-	1|1	5|6	1|3	2|7	2|2	17|18	5|8
TBC	-	-	1|1	14|28	1|2	3|6	2|2	17|18	4|5
TBR	-	-	1|1	2|4	1|2	3|6	2|2	17|18	4|10
BBL	-	-	-	4|5	-	1|3	2|2	13|15	4|7
BBC	-	-	-	17|25	-	1|3	2|2	13|15	1|2
BBR	-	-	-	2|2	-	1|3	2|2	13|15	5|11
TAL	1|1	-	-	8|42	-	2|2	3|3	14|15	15|30
TAC	1|1	1|3	-	10|72	-	2|2	2|2	14|15	9|32
TAR	-	-	-	9|34	-	2|2	3|3	14|15	16|30
BAL	-	-	-	4|19	-	1|1	1|2	11|12	9|20
BAC	-	-	1|1	8|55	-	1|1	1|2	11|12	12|23
BAR	-	-	-	10|18	-	1|1	1|2	11|12	8|15
AV%	100	33	100	30	43	54	88	92	48

had a success rate of only 30% . Bleeders were predicted only 43% of the time. Deep and uneven oscillation marks were predicted with a success rate of 54 and 88 % respectively on average and stopmarks were predicted with an accuracy of 92% . Depressions were predicted accurately on slabs by 48% .

Some of the "other inclusions" were predicted badly, probably due to a small defect passing between thermocouples (under-sampling of the thermocouples). The reason could also be that the operators were too conservative when making a measurement on other inclusions, thus including insignificant inclusions in the measurement. The inclusion could also have formed after the mould and even outside the casting machine. An example of this is when a slab has to be spot grinded because the slab was placed on a dirty floor, with the sheer weight of the slab making an impression of the dirt (resembling a "cleaned out" inclusion) on its surface. Deep and uneven oscillation marks and stopmarks were predicted in batches of three at the top before, top after, bottom before and bottom after locations. This is because the defects usually affect the whole width of the slab. Depressions were also not predicted accurately because 1575mm wide slabs are also included in the study, and thermocouples are not available near the off-corner of the slabs in this case, a location where the defect is predominant. Overall a conservative average accuracy of about seventy percent over all defects is achieved using the ARX technique as a predictor.

Also note between tables 3.11 and 3.12 that in some instances, such as stopmarks, when the prediction accuracy is high, the false alarm rate is also high. This implies that the method for determining the threshold is of such a nature that the increase in defect prediction accuracy results in an increase in the occurrence of the false alarm. This implies that, if it is desirable to detect when defects occur and some false alarms are allowed, the accuracy of positive defect prediction will also increase. Though more slabs will then have to be inspected before direct rolling or hot charging, more slabs can be direct rolled or hot charged because the slabs do not have to be grinded.

To ensure that the best possible result was obtained, the IVOV model was also trained using casting speed, mould level and inlet temperature as inputs. These results were however not an improvement on the current result. The reasons for not including the casting speed, mould level and inlet temperature in the IVOV model are described in §3.2.

3.4.4 Optimal set-points for IVOV system

With the IVOV model in hand, the next step is to determine which values for the thermocouple temperatures will yield the least amount of defects. These values then become set-points for a defect controller based on the MVIV model. For the smallest number of defects to occur, the best procedure was to assume that the system is at steady-state and then to calculate the values for the thermocouples which will deliver the least amount of defects. In the ARX formulation, the model is of the form[v]

$$\begin{aligned} \mathbf{p}[nT] &+ \mathbf{A}_1\mathbf{p}[(n-1)T] + \cdots + \mathbf{A}_5\mathbf{p}[(n-n_a)T] = \\ \mathbf{B}_0\mathbf{y}[nT] &+ \mathbf{B}_1\mathbf{y}[(n-1)T] + \mathbf{B}_2\mathbf{y}[(n-2)T] + \mathbf{B}_3\mathbf{y}[(n-3)T]. \end{aligned} \tag{3.12}$$

At steady-state, all inputs and all outputs are steady, so that

$$\begin{aligned} \mathbf{p}_{ss} &+ \mathbf{A}_1\mathbf{p}_{ss} + \cdots + \mathbf{A}_5\mathbf{p}_{ss} = \\ \mathbf{B}_0\mathbf{y}_{ss} &+ \mathbf{B}_1\mathbf{y}_{ss} + \mathbf{B}_2\mathbf{y}_{ss} + \mathbf{B}_3\mathbf{y}_{ss}. \end{aligned} \tag{3.13}$$

This implies then that at steady-state,

$$\begin{aligned} (\mathbf{I} &+ \mathbf{A}_1 + \cdots + \mathbf{A}_5)\mathbf{p}_{ss} = \\ (\mathbf{B}_0 &+ \mathbf{B}_1 + \mathbf{B}_2 + \mathbf{B}_3)\mathbf{y}_{ss}, \end{aligned} \tag{3.14}$$

and

$$\mathbf{p}_{ss} = (\mathbf{I} + \mathbf{A}_1 + \cdots + \mathbf{A}_5)^{-1}(\mathbf{B}_0 + \mathbf{B}_1 + \mathbf{B}_2 + \mathbf{B}_3)\mathbf{y}_{ss}, \tag{3.15}$$

To find a non-trivial solution to the above problem (*i.e.* find the values of $\mathbf{y}_{ss}$ s.t. $\mathbf{p}_{ss}$ are at least below the threshold values) one can use a search algorithm together with a least squares error to determine the values for the set-points of the thermocouple temperatures to ensure that no errors occur.

This has been done for the four models involved, and the resulting set-points are shown in Table 3.13 and graphically in Fig. 3.34.

The table and figure show that there is a distinct cooling pattern from the top thermocouple row of the mould to the bottom row. The variation between thermocouples, the non-symmetry (*e.g.* "ou4u", "ou5u", "in4u" and "in5u" are all symmetrically situated but do not have the same values) and the variation for different widths probably has to do with the contact that the thermocouple makes with the copper face. The set-points are based on a subset

[v] $\mathbf{y}$ are the thermocouple inputs (outputs of the MVIV model) and $\mathbf{p}$ are the defects (outputs of the IVOV model). Note that one sample delay has been incorporated into the inputs.

Table 3.13 Optimal temperature set-points, $\mathbf{r}(t)$ for the different MVIV models.

i	Thermocouple	1060mm	1280mm	1320mm	1575mm
1	in1u	104	105	107	104
2	in1l	95	96	100	95
3	in2u	108	107	109	108
4	in2l	95	98	101	95
5	in3u	107	105	109	107
6	in3l	94	93	97	94
7	in4u	106	106	109	106
8	in4l	95	94	92	95
9	in5u	102	105	107	102
10	in5l	94	97	94	94
11	in6u	106	110	109	106
12	in6l	102	103	102	102
13	in7u	108	108	109	108
14	in7l	100	100	99	100
15	in8u	114	105	117	114
16	in8l	106	101	113	106
17	nl1u	83	85	81	83
18	nl1l	80	83	80	80
19	nl2u	86	80	84	86
20	nl2l	75	74	72	75
21	ou1u	105	105	104	105
22	ou1l	92	94	97	92
23	ou2u	107	102	106	107
24	ou2l	99	92	103	99
25	ou3u	104	102	104	104
26	ou3l	94	95	96	94
27	ou4u	106	109	111	106
28	ou4l	90	94	94	90
29	ou5u	98	100	104	98
30	ou5l	93	95	96	93
31	ou7u	105	105	108	105
32	ou7l	97	90	98	97
33	ou8u	106	107	107	106
34	ou8l	96	98	97	96
35	nr1u	97	92	99	97
36	nr1l	90	86	94	90
37	nr2u	95	89	100	95
38	nr2l	86	83	91	86

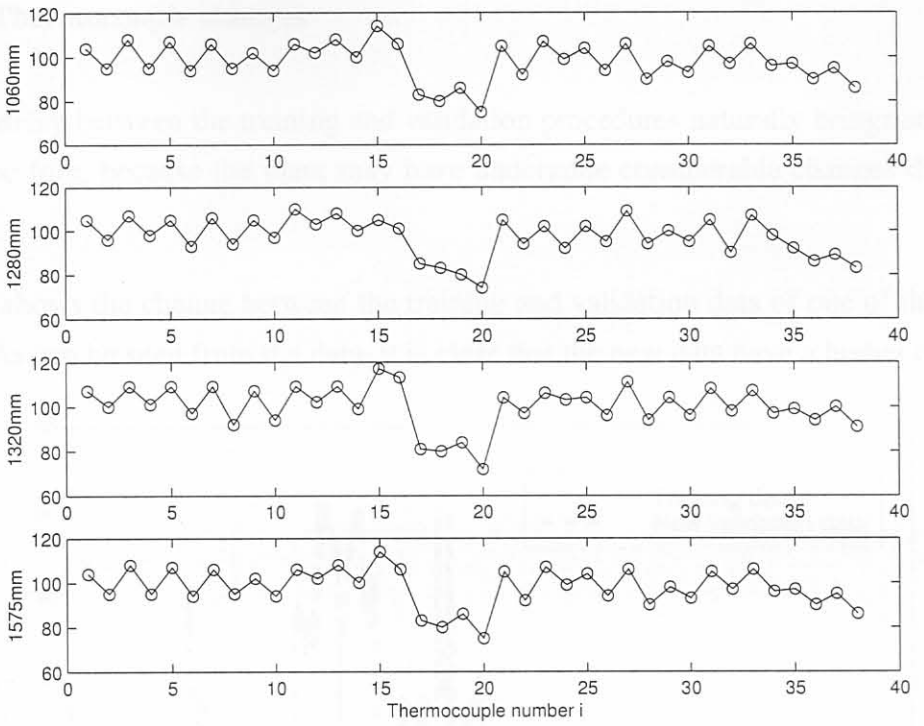

Figure 3.34 Graphical depiction of the optimal thermocouple temperature set-points for different slab widths.

of the occurring defects, and may not include all defects that will be present in the process in the future. However, it is assumed that these set-points will define a scenario which, if followed, can be considered to be the best process set-points for the thermocouple temperatures. Using the above set-points, the MVIV model can be used to derive the optimal casting speed, mould level and inlet water temperature in a similar fashion as was followed using the IVOV model to derive the optimal temperature set-points.

3.4.5 Preliminary validation of the IVOV model

All data gathered over the 6 month period was used to train the IVOV model (approximately 500 slabs), because the occurrence of defects was minimal. This left no more data to validate the IVOV model. To test whether the IVOV model was accurate, new data were gathered over a one-week period (44 slabs)—in the same way as the training data—almost three years after the initial model training procedure.

3.4.5.1 Thermocouple changes

The long delay between the training and validation procedures naturally brings some problems to the fore, because the plant may have undergone considerable changes during that period.

Fig. 3.35 shows the change between the training and validation data of one of the thermocouples. As can be seen from the data, it is clear that the new data have a higher offset than

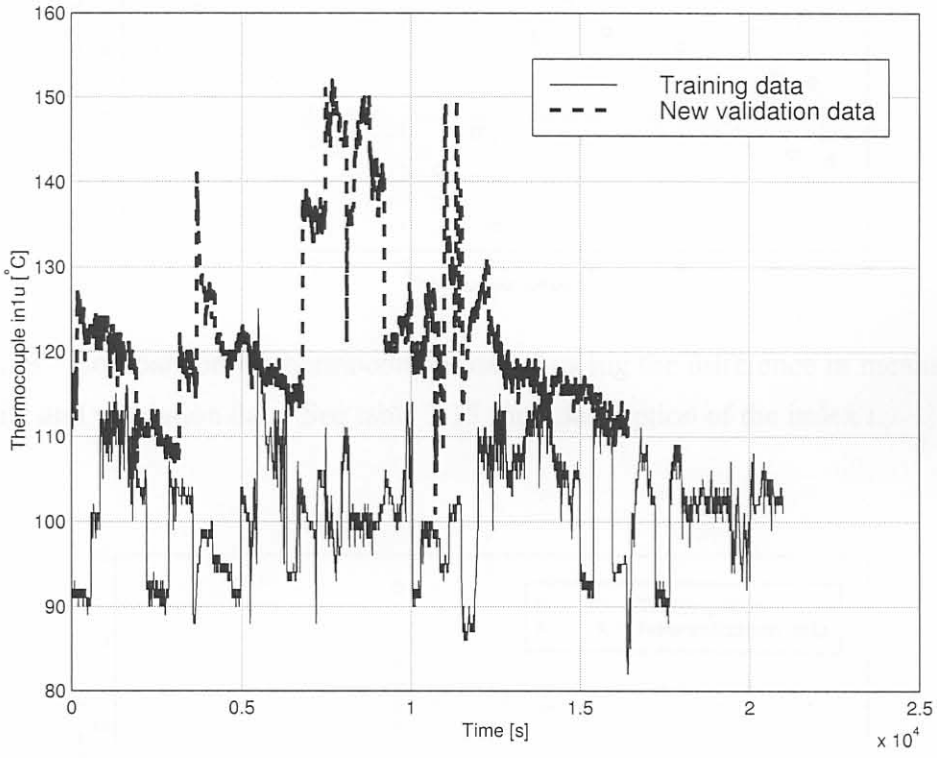

Figure 3.35 Comparison of data for thermocouple in1u showing the difference between the training and validation data.

the old data, and that the variation of the new data is more than that of the old data. This fact is highlighted in Fig. 3.36 and 3.37 which show the means and standard deviations of the various thermocouples for old and new data. On average, the means of the new data are about $15°C$ higher than the old data[w]; and up to $5°C$ difference in variance amplitude between the old and new data is observed(see especially *e.g.* thermocouple 15 which has much less variation in the new data than in the old data).

[w]Thermocouple 36 (nr11) was defective as can be seen from the lower mean and very high standard deviation. To compensate for this, the average of surrounding thermocouples was used to find proper values for the thermocouple.

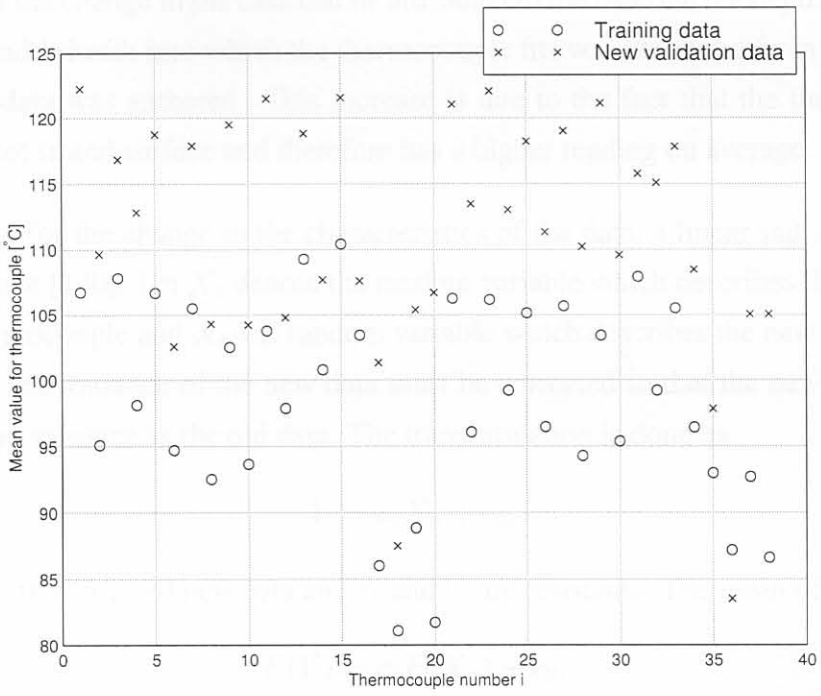

Figure 3.36 Comparison of thermocouple data showing the difference in means between the training and validation data. See table 3.13 for a description of the index i.

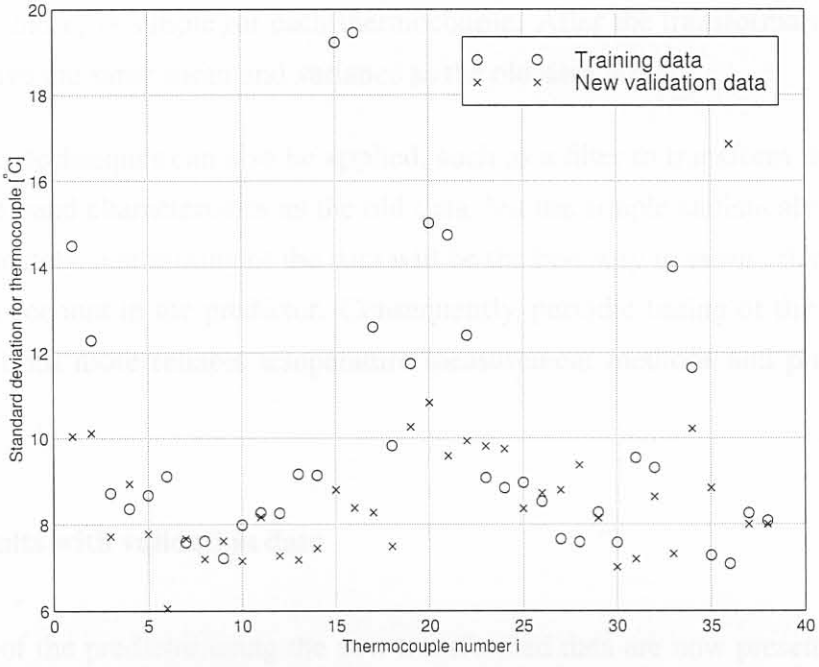

Figure 3.37 Comparison of thermocouple data showing the difference in standard deviations between the training and validation data. See table 3.13 for a description of the index i.

The reason for the change in the data can be attributed to the fact that the depth of the hole in the copper mould sheath into which the thermocouple fits was increased from 3mm to 5mm since the old data was gathered. This increase is due to the fact that the thermocouple is closer to the hot strand surface and therefore has a higher reading on average.

To compensate for the change in the characteristics of the data, a linear statistical transformation was done [140]. Let X_o denote the random variable which describes the old data for a specific thermocouple and X_n the random variable which describes the new data. Assume that the mean and variance of the new data must be corrected so that the new data have the same mean and variance as the old data. The transformation is done by

$$Y = c_1 X_n + c_2, \tag{3.16}$$

where Y is the transformed new data and c_1 and c_2 are constants. The mean of Y is given by

$$E(Y) = c_1 E(X_n) + c_2, \tag{3.17}$$

and the variance is given by

$$V(Y) = c_1^2 V(X_n). \tag{3.18}$$

Since the mean and variance of the new data must be equal to that of the old data, $E(Y) = E(X_o)$ and $V(Y) = V(X_o)$. This produces two equations with two unknowns and the solution of c_1 and c_2 is simple for each thermocouple. After the transformation of the new data, it will have the same mean and variance as the old data.

Note that other techniques can also be applied, such as a filter to transform the new data to have the same band characteristics as the old data, but the simple statistical transformation sufficed. Ultimately, a retraining of the data will be the best way to ensure that new changes are taken into account in the predictor. Consequently, periodic tuning of the predictor will be necessary until more reliable temperature measurement methods and practices can be implemented.

3.4.5.2 Results with validation data

Some results of the predictor using the new transformed data are now presented. Note that no transversal cracks or stopmarks occurred during the period when new data were gathered.

Fig. 3.38 shows the predictor output on the validation data for longitudinal cracking. Note that the threshold was implemented and that a value of 1 on the predictor output implies that a defect occurred and that a value of zero implies that the defect did not occur. 5 defects

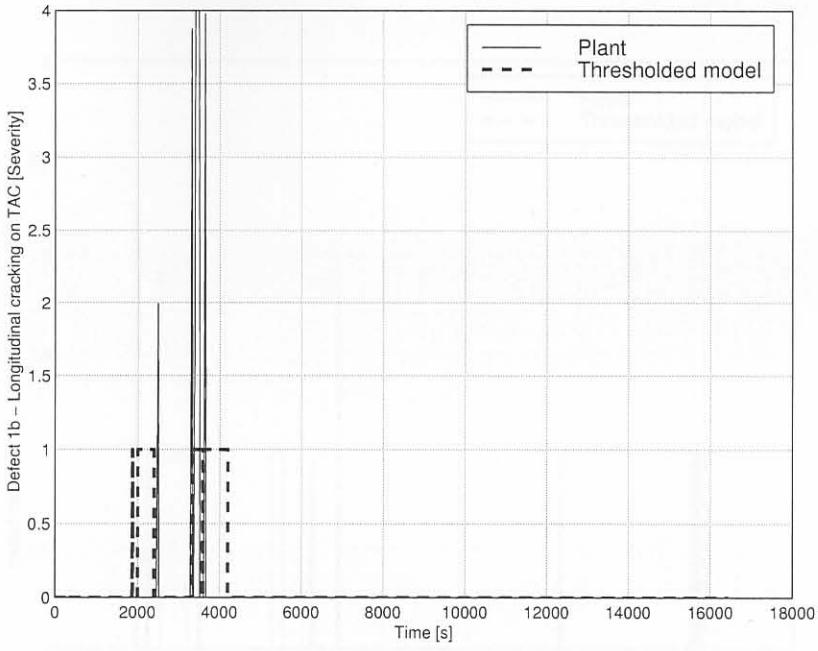

Figure 3.38 Comparison of predictor output and true plant data occurring at TAC position for longitudinal cracks.

occur, at $t \approx 2000$ to $t \approx 4000$ seconds. Note that the defect is predicted at $t \approx 2500$ seconds but the defect actually occurs just after the prediction. This is possibly a consequence of the 0.5 metre distance between defect samples on the slabs. During the period from $t \approx 3200$ to $t \approx 4100$ seconds the predictor indicates that defects occur, but the defect occurs only during a portion of this time. This could imply that the situation was favourable for a defect to occur, but that the defects simply did not occur over the period that the model predicted defects to occur.

Fig. 3.39 shows the occurrence of casting powder entrapment for the new data. Several defects occur, with a long period of defect occurrence from $t \approx 2000$ to $t \approx 3500$ seconds. During this period, defects were predicted, though not precisely at the same time as the defects occurred. The other defects which occurred but which were not predicted could have been deemed to be severe at the time of new data gathering and not at the time of old data gathering[x]. Note that towards the end a defect was predicted but did not occur ($t \approx 16000$ seconds), and may be due to an error in the HMS.

Fig. 3.40 and fig. 3.41 show the predictor outputs for other inclusions at the BBL and BAC locations respectively. Four defects are predicted and one defect actually occurs at the BBL location. Note that there is a slight delay between the defect being predicted and the defect

[x]Inspection of the slabs was performed by the author and some personnel at the steel-making company.

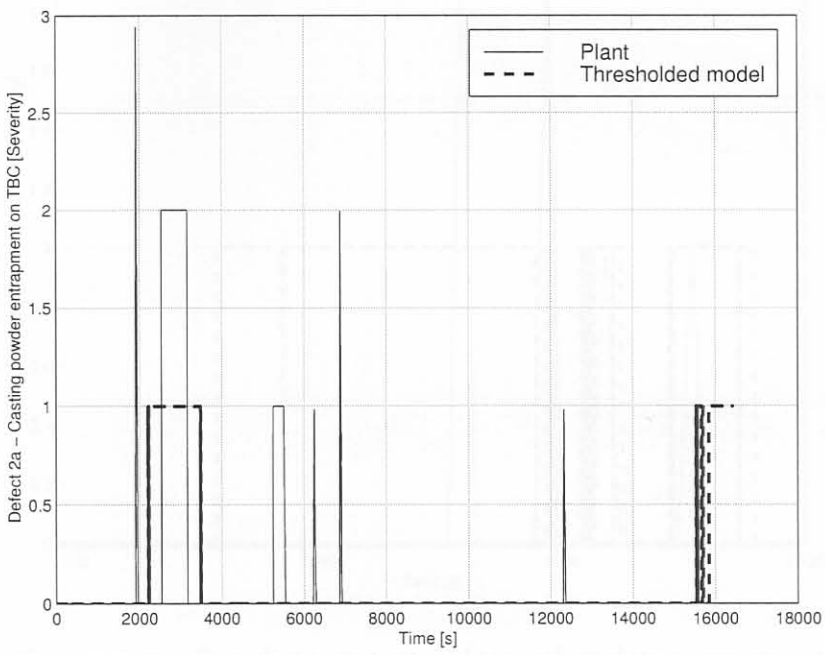

Figure 3.39 Comparison of predictor output and true plant data occurring at TBC position for casting powder entrapment.

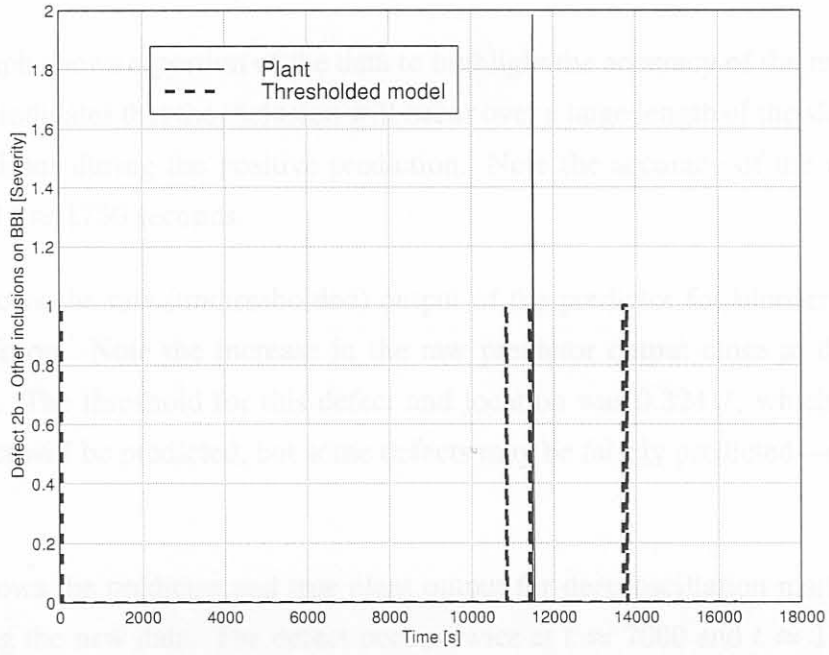

Figure 3.40 Comparison of predictor output and true plant data occurring at BBL position for other inclusions.

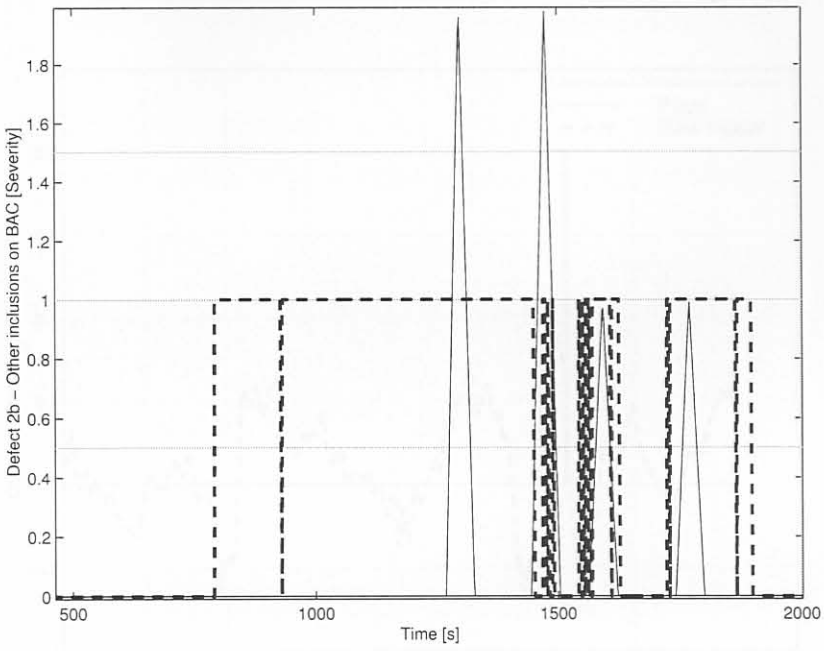

Figure 3.41 Comparison of predictor output and true plant data occurring at BAC position for other inclusions.

occurring at time $t \approx 11500$ seconds. The reason that defects were predicted but were not truly present in the other locations can probably be attributed to the HMS not noticing the defects.

The BAC graph shows a portion of the data to highlight the accuracy of the model. Though the predictor indicates that the inclusion will occur over a large length of the slabs, the defect occurs four times during the positive prediction. Note the accuracy of the model at time $t \approx 1600$ and $t \approx 1750$ seconds.

Fig. 3.42 shows the raw (unthresholded) output of the predictor for bleeders occurring at the TBL position. Note the increase in the raw predictor output close to the occurrence of the defect. The threshold for this defect and location was 0.3241[y], which would imply that the defect will be predicted, but some defects may be falsely predicted—due to the low threshold.

Fig. 3.43 shows the predictor and true plant output for deep oscillation marks at the TBL location using the new data. The defect occurs twice at $t \approx 7000$ and $t \approx 11500$ seconds. Note that a value of 0.5 on the predictor indicates a defect to avoid ambiguity with the plant outputs. The defect at $t \approx 7000$ seconds is predicted and the defect at $t \approx 11500$ is not. This

[y] see table G.1 for the threshold values used for 1060mm wide slabs like the one where this defect occurs.

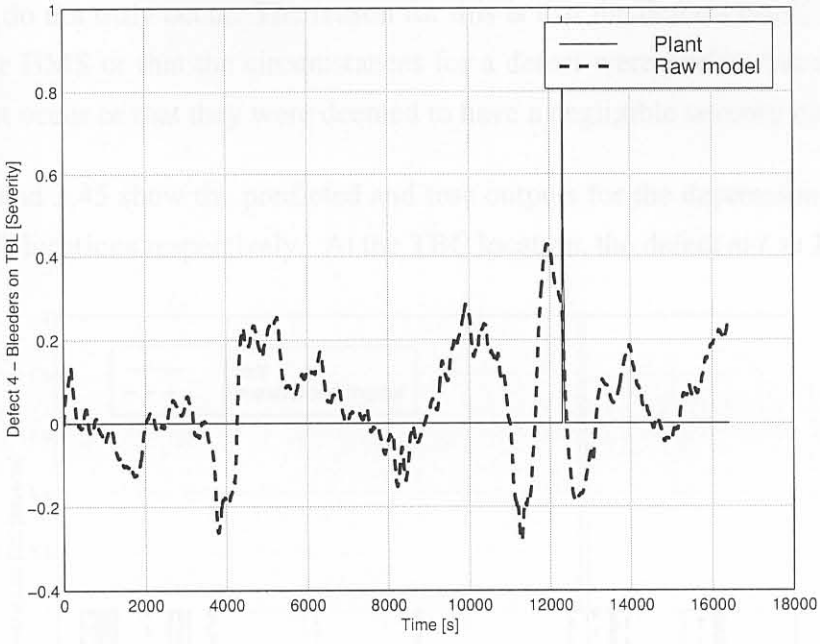

Figure 3.42 Comparison of predictor output and true plant data occurring at TBL position for bleeders.

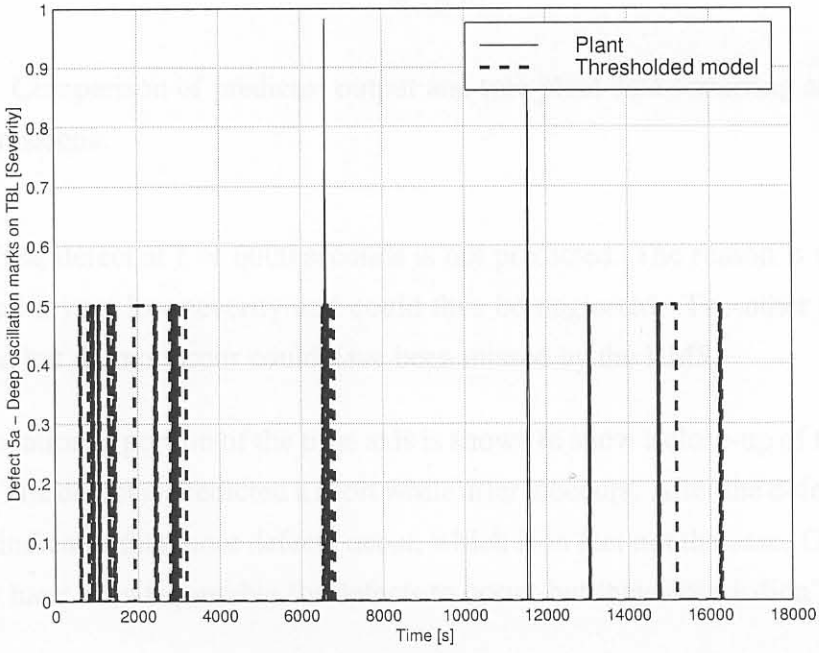

Figure 3.43 Comparison of predictor output and true plant data occurring at TBL position for deep oscillation marks.

could be due to the defect being characterised inaccurately. Furthermore, several defects are predicted but do not truly occur. The reason for this is that the defects could not have been noticed by the HMS or that the circumstances for a defect were perfect but that the defect simply did not occur or that they were deemed to have a negligible severity by the HMS.

Figures 3.44 and 3.45 show the predicted and true outputs for the depression defects at the TBC and BBR locations respectively. At the TBC location, the defect at $t \approx 13000$ seconds

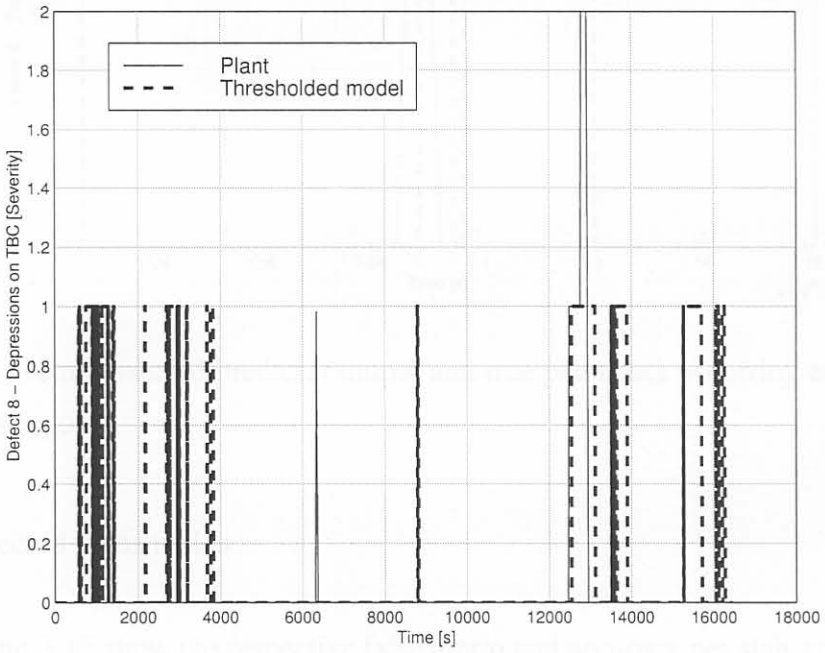

Figure 3.44 Comparison of predictor output and true plant data occurring at the TBC position for depressions.

is predicted. The defect at $t \approx 6000$ seconds is not predicted. The reason is that the defect could have had a very low severity and could thus be neglected. The other defects which were predicted but did not occur could have been missed by the HMS.

At the BBR location, a portion of the time axis is shown to show a close-up of the occurrence of the defect. The defect is predicted a short while after it occurs. After the defect is predicted the predictor indicates that more defects occur, which is in fact not the case. Once again, the situation may have been favourable for defects to occur, but they simply didn't.

Other defect predictions are not shown due to constraint of space, though similar results were obtained.

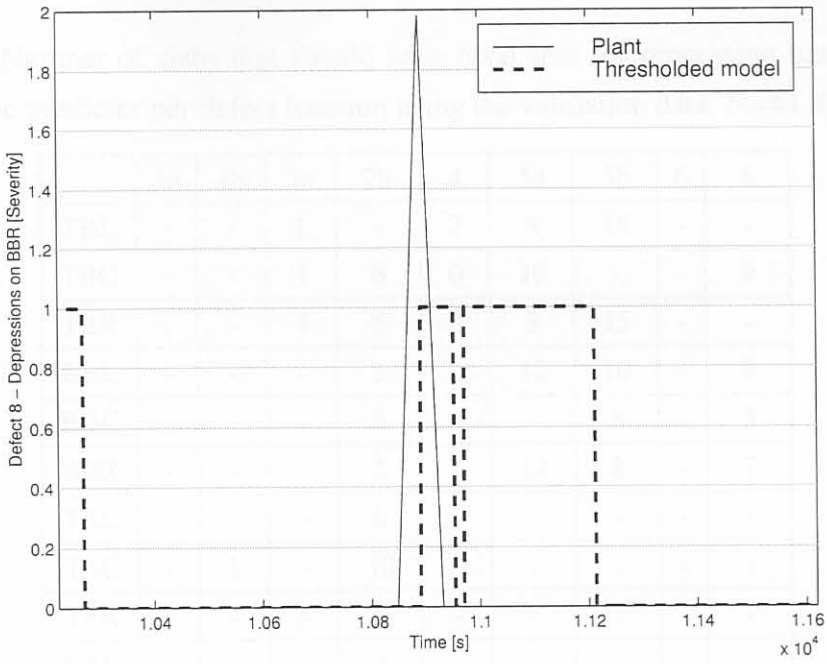

Figure 3.45 Comparison of predictor output and true plant data occurring at the BBR position for depressions.

3.4.5.3 Defected slabs ratios

Tables 3.14 and 3.15 show the respective false alarm and accuracy per slab grinded, respectively, similar to the tables obtained during the training phase (see tables 3.11 and 3.12).

False alarms on one slab was given and the accuracy of defect prediction was 100% for longitudinal cracking. This is impressive since the training data show that the predictor was only 33% accurate. Casting powder entrapment had a decrease in the number of false alarms over that of the training data. The accuracy dropped however considerably from 100% to 30% . This is probably because the defects can pass between two thermocouples. For other inclusions, the number of false alarms in the cases of the training and validation data are comparable at 16% and, through coincidence, the number of accurate defect predictions improved from 30 to 48% in the respective cases. Bleeders had a tenfold increase in the number of false alarms, and a decrease in the amount of accurate predictions. Both types of oscillation marks had an increase in the number of false alarms. Deep oscillation marks improved in accuracy from 54 to 63% and uneven oscillation marks reduced from 88 to 25% . Depressions had the same percentage of false alarms in both cases and an increase in the accuracy of the predictions per slab from 48% to 67% .

The conservative 95% confidence intervals for slabs with defects and positive predictions can

Table 3.14 Number of slabs that should have been sent for processing based on a false alarm from the predictor per defect location using the validation data. N=44 slabs.

	1a	1b	2a	2b	4	5a	5b	6	8
TBL	-	-	1	-	7	8	15	-	-
TBC	-	-	1	6	0	10	-	-	9
TBR	-	-	4	5	0	9	15	-	-
BBL	-	-	-	3	-	12	10	-	9
BBC	-	-	-	8	-	-	8	-	3
BBR	-	-	-	5	-	12	8	-	7
TAL	-	-	-	6	-	-	-	-	-
TAC	-	1	-	10	-	-	-	-	-
TAR	-	-	-	9	-	-	-	-	-
BAL	-	-	-	3	-	-	-	-	-
BAC	-	-	-	17	-	-	-	-	-
BAR	-	-	-	5	-	-	-	-	-
AV%	-	2.3	4.5	16.0	5.3	23.0	25.0	-	15.9

Table 3.15 Number of slabs that should have been sent for processing based on the predictor where a slab was truly defected using the validation data. N=44. In $x|y$, x is the number of slabs predicted to have the defect and y is the number of slabs that did have the defect present.

	1a	1b	2a	2b	4	5a	5b	6	8
TBL	-	-	1|2	-	1|1	1|2	1|1	-	-
TBC	-	-	1|6	1|1	0|2	2|3	-	-	1|2
TBR	-	-	1|2	1|1	0|1	1|2	1|1	-	-
BBL	-	-	-	1|1	-	1|2	0|2	-	1|2
BBC	-	-	-	1|2	-	-	0|1	-	1|1
BBR	-	-	-	0|1	-	5|7	0|3	-	1|1
TAL	-	-	-	1|3	-	-	-	-	-
TAC	-	2|2	-	1|4	-	-	-	-	-
TAR	-	-	-	2|3	-	-	-	-	-
BAL	-	-	-	4|11	-	-	-	-	-
BAC	-	-	-	6|8	-	-	-	-	-
BAR	-	-	-	2|7	-	-	-	-	-
AV%	-	100	30	48	25	63	25	-	67

Table 3.16 Overall conservative 95% confidence intervals on slabs with defects versus slabs that were predicted to have defects.

Defect	Confidence interval
Transversal cracks	$100 < p < 100$
Longitudinal cracks	$17 < p < 100$
Casting powder entrapment	$19 < p < 73$
Other inclusions	$28 < p < 37$
Bleeders	$7 < p < 65$
Deep oscillation marks	$43 < p < 70$
Uneven oscillation marks	$59 < p < 88$
Stopmarks	$88 < p < 96$
Depressions	$41 < p < 55$

be found in table 3.16. These values were calculated using both the training and validation sets where available, because of the few occurrences of defects. Transversal cracks do not have a true confidence interval since the proportion is close to 1. Longitudinal cracks can be up to 100% accurate as was seen with the validation data. Stopmarks seem to fair the best and other inclusions fair the worst.

3.4.5.4 Comparative results

For comparison, the only paper found on the prediction of defects with quantified results is by Hunter *et al.* [18]. Hunter *et al.* [18] use a feed-forward artificial neural network to predict defects from mould variables (including thermocouple temperature measurements). Table 3.17 shows the results of the ARX predictor per defect using the training and validation sets together where available. The calculation of the accuracy is based on predictions per *sample point*. The *sensitivity* is the proportion of correctly predicted sample points to all the sample points where a defect truly occurs. The *specificity* is the proportion of unpredicted defect points to the number of points where defects truly do not occur. The *false alarms* (FA) is the proportion of predicted defect points to the number of points where defects truly do not occur (FA=1-specificity). The *positive predicted value* (PPV) is the number of correct predictions of defects being present to the total number of predictions that the defects are present. The *negative predicted value* (NPV) is the number of correct predictions of defects not being present to the total number of predictions that defects are not present. N is the number of sample points used. Note that this method is conservative if the only consideration is whether

Table 3.17 Accuracy of the ARX predictor using sensitivity.

Defect	Sensitivity	Specificity	FA	PPV	NPV	N
Transversal cracks	73.4	99.5	0.5	51.7	99.8	20998
Longitudinal cracks	63.6	93.5	6.5	16.3	99.2	8212
Casting powder entrapment	8.8	98.6	1.4	4.9	99.3	61768
Other inclusions	24.8	96.6	3.4	13.1	98.4	1171032
Bleeders	14.4	100.0	0.0	98.5	99.6	114027
Deep oscillation marks	42.3	98.7	1.3	12.4	99.7	931428
Uneven oscillation marks	66.3	99.4	0.6	43.0	99.8	740832
Stopmarks	41.3	94.8	5.2	13.0	98.9	509064
Depressions	44.8	96.3	3.7	13.7	99.3	1168272

a slab must be grinded or not.

The result that is given in the paper of Hunter *et al.* [18] is that of the validation set for longitudinal cracking, where a neural network output generates a sensitivity of 61.5% and specificity of 75% . The table shows that the respective values using the ARX methods are 63.6% and 93.5% [z]. This implies that the ARX predictor is marginally more accurate than that published in terms of correct predictions of defects. The specificity however shows that many false alarms occur in the results of the paper, while the ARX predictor has far fewer false alarms (0.5%). An allowed decrease in specificity should also increase the sensitivity. This can be achieved by lowering the threshold. Transversal cracks have the best overall performance, with a sensitivity to predict a crack of 73.4% . Casting powder entrapment fairs the worst with a sensitivity of 8.8% and a PPV of 4.9% . There are however few false alarms (1.4%). Other inclusions have a correct prediction when defects occur over the sample points of nearly 25% . Bleeders have no false alarms, but have low sensitivity. Deep oscillation marks have a sensitivity of 42.3 % and very few false alarms (1.3%). Uneven oscillation marks also have high sensitivity (66.3%) and specificity (99.4%). Stopmarks have a sensitivity of 41.3% and 94.8% specificity so the amount of alarms are low. Depressions have similar sensitivity at 44.8% and specificity of 96.3 %. Overall, the data show that the predictor has few false alarms, but is also not always very accurate. However, comparative results could not be found for other defects.

The predictor of the defects was derived in this section with good results using ARX tech-

[z]Note that the longitudinal values are based on the validation set for comparison. Transversal cracks and stopmarks are based on the training set because none of these defects occurred during the validation phase.

niques together with a threshold. Not all the graphical results could be shown for each of the defects due to space constraint. The IV to OV model can not only be used as a predictor of defects, but in an inversion it can be used to determine the best thermocouple temperature set-points so that no defects occur.

3.5 Conclusion

This chapter presented the methodology and results of a model that can be used for prediction and control of defects in the continuous casting process.

The data gathering procedure of the mould variables (inputs) and the defects (outputs) was described. The inputs are available form the level 2 system of the plant of the industrial partner in real time and the defects are measured by experienced operators several hours after casting of a slab is completed. The procedure to extract the relevant data from the vast amount of data collected from the plant was also described.

Using statistical hypothesis testing and correlation analysis, it was found that the model can be divided into two sub-models. The first model, here called the MV to IV model, describes the dynamic effect of casting speed, as a manipulated variable, and mould level and inlet temperature as two possible disturbances, on the thermocouple temperatures as outputs. The second model is called the IV to OV model and uses the thermocouple temperatures as inputs and the defects as outputs. The IV to OV model is the predictor of the defects. This is convenient as feedback control can now be used because the time delay caused between measurement of the defect and the actual occurrence of the defect is outside the control loop.

The training of the two models was also presented. Both models track the true plant outputs well. System identification techniques in the form of linear auto-regression with exogenous input was found to be a just way to model the process. The IV to OV model could not determine the severity of the defects, but the use of a threshold improved the predictor to the extent that it could tell when and where a defect occurs and which defect was present with relatively high accuracy. Validation data for the IVOV model were not available, due to the comparatively few defects that occurred. Data collected three years later were used to validate the IV to OV model, and the obtained results compare favourably to published results for longitudinal cracking. The MV to IV model was relatively accurate in the presence of noise, even on the validation data.

The IV to OV model can be used in an inverse problem to determine the best temperature set-points for the thermocouples such that no defects occur. These results were shown.

The MV to IV model can now be used to design controllers in a feedback fashion so that the thermocouple temperature set-points can be followed. This is the subject of the next chapter.